CONFIDENTIAL

ST. ANTHONY FALLS HYDRAULIC LABORATORY
UNIVERSITY OF MINNESOTA

Project Report No. 52

EXPERIMENTAL STUDIES OF A HYDROFOIL DESIGNED FOR SUPERCAVITATION

Submitted by
LORENZ G. STRAUB
Director

Prepared by
JOHN F. RIPKEN

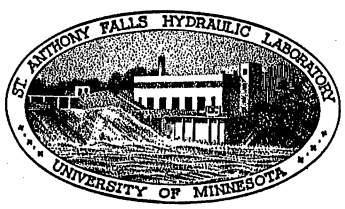

September 1956

Prepared for the
OFFICE OF NAVAL RESEARCH
Department of the Navy
Washington, D. C.
Under Office of Naval Research Contract N6onr-246 Task Order VI

CONFIDENTIAL

PREFACE

The 10-in. free-jet water tunnel at the St. Anthony Falls Hydraulic Laboratory was developed under a study program sponsored by the Office of Naval Research in contract with the University of Minnesota.

This report discusses the use of the facility in determining the test performance characteristics of a family of hydrofoils which have been specifically designed for operation under conditions of extreme cavitation. These studies are one phase of a supercavitating hydrofoil program initiated by the Office of Naval Research. This report is interim in that the studies are continuing.

This report was prepared by John F. Ripken with general assistance by Alexander B. Rudavsky. Edward Silberman and Joseph W. Wetzel contributed in the analytical phases. Loyal A. Johnson, assisted by Eileen M. Potter, edited the manuscript.

The study was conducted under contract N6onr-246. Task Order VI.

ABSTRACT

Thin hydrofoils specifically designed to operate under conditions of extreme cavitation have been tested in a free-jet water tunnel to determine their performance characteristics in two-dimensional flow.

The hydrodynamic forces acting on the foil section were evaluated from pressure distribution measurements, and related cavitation observations were made.

The force studies indicated favorable performance but established the necessity for providing a very thin and sharp leading edge. The small rounding of the leading edges tested obscured possible correlation with the basic theory of the foil design employed.

CONTENTS

LIST OF ILLUSTRATIONS

EXPERIMENTAL STUDIES OF A HYDROFOIL DESIGNED FOR SUPERCAVITATION

1. INTRODUCTION

Hydrofoils employed as propeller blade elements or lifting surfaces are normally designed to provide a favorable lift-to-drag ratio or optimum performance when operating under essentially non-cavitating conditions. Operation of such hydrofoils under conditions causing steady (or quasi-steady) cavitation produces a very unfavorable low lift and high drag performance. The steady state cavitation referred to here differs from the more common small transient cavitation in that the cavity is more nearly steady and the cavity length is at least a large fraction of the body length.

Since performance objectives continually tend toward greater relative speeds in hydrofoil applications, and since known design practice cannot suppress cavitation on foils moving with high speed at shallow depth, it becomes apparent that foil operations with extensive cavitation will tend to be considered more normal than exceptional. In light of this, an appropriate design practice is sought which will basically provide an optimum performance under conditions involving extensive cavitation.

Tulin and Burkart [1]*, employing hydrodynamic analysis, determined profiles for a hydrofoil family intended to operate with a minimum drag under supercavitation (cavity of infinite length or $\sigma = 0$)** conditions. These foils have a line profile with coordinates defined by the equation

$$y/S = [4\ C_{L_d}/5\pi\ ][(x/S) + 8/3\ (x/S)^{3/2} - 4\ (x/S)^2]$$

where C_{L_d} is the selected lift coefficient of the section when operating under design conditions and S is the foil chord length.

The coordinate axes, orientation, and cavity disposition of such a foil are schematically depicted in Fig. 1. It should be noted that the theory

---

*Numbers in brackets refer to the List of References on p. 16.

**For a definition of the cavitation parameter, σ, see p. 8.

assumes an infinite flow field, flow entering tangential to the lower surface, stagnation occurring on the leading edge, and the cavitation number $\sigma = 0$. The orientation, consistent with these design conditions, has been arbitrarily defined by $\alpha' = 0$ where α' denotes the angle between the x axis and the axis of the flow field. Theoretically, operations at or above the ideal angle $\alpha' = 0$ will be free of cavitation on the lower foil surface, while operations at lower angles may cavitate from the lower surface. Presumably, if the foil is operated at other than the ideal angle, the lift-to-drag ratio will be reduced below the selected design value.

This report describes experimental studies of two simulated members of the Tulin-Burkart family of foils, with the objective of determining their performance characteristics under a range of cavitating and non-cavitating two-dimensional flow conditions and a range of angles of attack.

The report briefly describes the test facilities and the simulated profiles tested. The resulting foil pressure distribution measurements and cavitation observations are then summarized and examined relative to the theory and to other available foil test data.

II. THE TEST FACILITY

The flow field imposed on the test hydrofoils during the experimental studies was provided by the free-jet water tunnel facility [2] available at the St. Anthony Falls Hydraulic Laboratory. This tunnel had a test stream of 10-in. diameter in which the water flowed vertically downward through a "free" (gas-enveloped) test section. The stream velocity was variable from about 25 to 50 fps, and the pressure in the test stream could be varied by varying the pressure in the chambered gas enveloping the jet. The pressure could be varied from atmospheric to nearly vapor pressure.

A single curved viewing-window contacted the periphery of the jet through a peripheral arc of 45 degrees and extended axially downstream of the tunnel contraction for a distance of 38 inches.

The water employed was untreated Mississippi River water which flowed through the tunnel by gravity without recirculation. The water temperature and clarity varied with the season, but the bulk of the test data was obtained in the winter months when the clarity was excellent and temperatures were

about 33 F. The water contained a small amount of solid contamination and was assumed to have a normal or nearly saturated gas content.

The tunnel was uniquely adaptable to the supercavitating tests because of an inherent ability to operate at σ values as low as 0.009.

The velocity distribution in the undisturbed test stream was established as uniform within 1.0 per cent over the central 95 per cent of the diameter and measurements with a turbulence sphere established a critical Reynolds number of 200,000. During the tests the value of the Reynolds number, based on foil chord, varied from approximately 250,000 to 500,000.

III. THE HYDROFOIL TEST ASSEMBLIES

The basic foil equation permitted selection of an infinite number of specific profiles depending on the arbitrary selection of a design lift coefficient C_{L_d} and chord length S. For the purpose of these tests, values of $C_{L_d} = 0.3$ and $C_{L_d} = 0.5$ were selected. The smaller of these two values represents a foil of about 3.5 per cent maximum camber and the larger about 6 per cent. The coordinates of the profiles are shown in Table I, and scale profiles are shown in Figs. 2 and 20.

Table I - Profile Data for the Test Hydrofoils

x/S	0	0.10	0.20	0.30	0.40	0.47	0.50	0.60	0.70	0.80	0.87	0.90	1.00
y/S for C_{L_d}=0.3	.0000	.0110	.0212	.0288	.0332	.0340	.0338	.0306	.0231	.0114	.0000	- .0048	- .0254
y/S for C_{L_d}=0.5	.0000	.0183	.0354	.0480	.0554	.0567	.0564	.0510	.0386	.0190	.0000	- .0080	- .0424

The foil chord length, S , was selected as 2.5 inches. This size constituted a compromise between the need for a model which would be large enough to permit practical construction of the necessary internal pressure tap system, yet small enough to operate in the 10-in. diameter test stream without excessive distortion of the field. The allowable foil size from the standpoint of distortion was indeterminate on the basis of either prior experience or an analytical determination. Thus, the final selection of 2.5 in. was arbitrary.

The theory relating to the determination of the foil profile pertains only to the coordinates of the concave face for the condition $\sigma = 0$, with

the presumption that cavitation originates at the leading edge and completely envelopes the convex surface as shown in Fig. 1. While neither the Tulin-Burkart theory, nor other analytical approaches, permitted a practical determination of the coordinates of the cavity surface for various σ and α' values, it was evident that minimum foil drag would be associated with cavities of minimum relative thickness. This, in turn, required that the foil be of minimum thickness to assure that the resulting cavity originated only from the concave face and not as a result of water contact on the convex face.

In view of these conditions, a design study was conducted for the purpose of evolving a two-dimensional test foil which would have the desired minimum thickness, a high profile accuracy, adequate structural strength, and a workable pressure tap system. The compromise fabrication which was finally adopted was composed essentially of tensioned steel strands lying parallel and side by side while supported by two mounting blocks shaped to the profile of the selected foil. The individual strands formed a corrugated surface which was fused into a smooth sheet by application of soft solder.

The basic accuracy of the foil was established by the shaped mounting blocks over which the strands were strung. These blocks were machined and oriented to the selected coordinates by a standard milling machine traversed in step increments in accord with the layout depicted in Figs. 2 and 3. The selected step width, dx , was made to correspond to the diameter of the stranding used, and the step height, dy , was varied in accord with the profile equation.

In the first foil ($C_{L_d} = 0.5$) the strands were of 0.026-in. diameter music wire interspersed with stainless steel tubes of 0.025-in. diameter and 0.006-in. wall thickness.

In the second foil ($C_{L_d} = 0.3$) the strands were increased to an outside diameter of 0.035 in. and all strands consisted of tubing rather than a mixture of wires and tubes. This stranding modification reduced the pressure transmission difficulties encountered with the smaller tubing and permitted a better distribution of pressure taps.

The foil assembly was made in a jig which fixed the position of the template blocks and individually tensioned each of the strands to about 15 lbs. with a spring loading. The solder was then flowed on and scraped off tangent to the strands to form a unified smooth flow surface. The pressure taps were

then drilled (0.0135 in.) normal to the surface near the center of the span and the outer ends of the tubes were provided with external connections for attachment to the manometer lines. The entire assembly was then transferred to an external yoke (shown in Fig. 4) which was precompressed to continually maintain a stiffening tension in the stranding. The dimensions of this yoke were selected to permit supporting the foil along a diameter of the 10-in. test stream with the yoke encircling, but not contacting, the stream.

Two parallel flow-splitter plates (shown in Fig. 4a)were then attached to the yoke and the foil in a manner that would produce a two-dimensional flow, reduce the structural foil span, and would prevent spanwise access of air to the test region during operation.

The entire assembly, as shown in its normal position in Fig. 4a, was suspended in the tunnel test section by a trunnion mounting with the axis horizontal and parallel to the foil axis. The assembly was rotated about this axis by a worm-gear mechanism with controls external to the tunnel test section. With this mechanism, the angle of attack, α', of the stream on the foil could be varied from -5 to +10 degrees, with a setting accuracy of about 1/10 degree.

In the initial studies with the foil of $C_{L_d} = 0.5$ and thickness 0.026 in., it was felt that the flow field would be primarily influenced, in accord with the theory, by the configuration of the concave surface. It was assumed that the influence of the leading edge, which was a half cylinder with diameter approximating 1.0 per cent of the chord, would be relatively local and unimportant. The error of this assumption was not disclosed by the early tests which were terminated at a minimum $\sigma = 0.14$ for fear of structural failure of the assembly; however, subsequent construction and test of the thicker and stronger foil with $C_{L_d} = 0.3$ and thickness, 0.035 in., established that the leading edge exerted dominant cavitation flow control when σ was reduced to small values (0.10 to 0.01).

In an experimental effort to reduce the adverse character of the cavity shed by the cylindrical leading edge, a number of geometric alterations were made in the edge. These were of a preliminary nature and were restricted to simple changes of the existing edge structure. The three alternates which were tested are shown in Fig. 5.

IV. THE TEST PROCEDURES

The measurements represented by the tests include undisturbed stream velocity V_o, absolute undisturbed stream pressure P_o, water temperature T, local absolute pressure measurements on the foil P, and the foil angle of attack α'.

The stream velocity V_o was measured by calibrated pressure differentials existing in the contraction cone of the tunnel, located just upstream of the test foil. The velocity was controlled by a combination of settings on two valves in the tunnel main-flow circuit.

The undisturbed stream pressure P_o in a free-jet type of water tunnel is assumed to be the same as that of the chambered gas which surrounds the liquid jet. The differential pressure between this chamber and the atmosphere external to the tunnel was measured with a mercury manometer and compensated for the existing barometric pressure. The pressure was controlled by a combination of settings on the two main-flow control valves, plus a valve which bled air into the gas chamber from the atmosphere.

In the test tunnel the gas surrounded free-jet passes from the test chamber into a water-filled discharge pipe. The plane of abrupt jet expansion at the downstream end of the gas chamber is controllable in vertical position relative to the test foil. In the bulk of the tests described herein the jet expansion was positioned well below the test foil. However, in certain high angle tests with the larger cambered foil ($C_{L_d} = 0.5$) it was necessary to raise the level of the expansion or backwater until it approached the trailing edge of the foil. This flooding was necessary to prevent splitting of the jet by the foil assembly.

A split jet operation in a free-jet tunnel has sometimes been employed as an approximation of the flow condition $\sigma = 0$. In these tests split jet operation was considered to introduce obscure secondary flows and was avoided by providing tail water flooding as described.

The water temperature, T, was measured by an immersion thermometer inserted through the tunnel boundary upstream of the contraction.

Each of the pressure taps in the foil surface transmitted its particular pressure through the stainless-steel tubing strands, connected plastic tubing, and thence to an external mercury manometer. The manometer was of

the differential type, with the second leg connected to the chambered gas surrounding the test stream. In view of the gassing and time-lag difficulties associated with using water-filled pressure transmission lines for low vacuum measurements, the lines were filled with gas during the measuring procedure. This presented no problem with the manometer leg connected to the chambered gas in the tunnel test section, but in the other leg it necessitated maintaining a gas-water interface at the pressure tap point on the foil surface. This was accomplished by forcing compressed air into the manometer line until bubbles streamed from the tap and the mercury in the manometer was displaced more than during the subsequent test reading. Stoppage of the compressed air supply then resulted in a gradual settling back of the manometer and cessation of streaming bubbles at the tap. The eventual settled reading of the manometer was considered to be the measure of the dynamic pressure existing on the foil. A slight correction was subtracted from this reading to account for the surface-tension effect existing at the gas-water interface in the small hole. This was statically measured and found to be equivalent to 4 in. of water head.

The angle of attack of the foil α' was initially set with the axis of the fabrication parallel to the tunnel axis.

V. THE TEST DATA

The preliminary foil experimental studies described herein were restricted to pressure distribution measurements on the foil surface and visual and photographic observations of the accompanying cavitation.

In the tests of the foil with $C_{L_d} = 0.5$, angles of attack of $\alpha' = -4, -2, 0, +2, +4,$ and $+6$ degrees were employed with a stream velocity, V_o, varying from 30 to 40 fps. The bulk of the tests were run at 40 fps and the pressure, P_o, was varied to provide a non-cavitating condition of $\sigma = 1.61$ and cavitating conditions of $\sigma = 0.21$ and $\sigma = 0.14$.

In the tests of the foil with $C_{L_d} = 0.3$, the range was extended with $\alpha' = -4, -2, 0, +2, +4, +6, +8,$ and $+10$ degrees while V_o varied from 25 to 49.5 fps. Pressure P_o was varied to provide a non-cavitating condition of $\sigma = 2.31$, and cavitating conditions of $\sigma = 0.28, 0.12,$ and 0.01.

The pressure readings are presented in the form of the local value of the dimensionless pressure coefficient $(P/W - P_o/W)/V_o^2/2g$, and the tap positions were sufficiently dispersed to provide a fairly comprehensive con-

cept of the pressure distribution. The steep pressure gradients near the leading and trailing edges were not clearly defined, but any errors involved in their estimate were not deemed significant in the evaluations of the lift force.

Detailed average pressure distribution data are shown in Figs. 6 through 13 for various angles of attack α'. The averaged plottings do not show the data scatter, but it was observed in the data handling that considerable scatter did occur in certain areas. In general, such areas correlated well with those in which either flow separation transients or the effects of transient cavitation might be expected to exist.

The evaluations of the cavitation index σ are based on the form $\sigma = (P_o/W - P_v/W)/V_o^2/2g$. In this, P_o/W is again the absolute stream pressure head while P_v/W is the vapor pressure head in feet of water for fresh water at the measured temperature, T .

On the basis of the foregoing definitions, it is apparent that the lowest obtainable value of the pressure coefficient will be a negative one approximating the absolute value of the concurrent cavitation σ . Evidence of this pressure concurrence serves as an indication of the presence of cavitation and was consistently verified by visual observations of cavitation during the tests. It is to be noted, however, that the concurrent pressures are only approximately equal, with the measured pressures generally being somewhat greater than the vapor pressure and with the difference increasing as σ increases. This same trend has been observed in other cavity studies [3] and [4] and is attributed to the presence of gases being released to the cavity by the liquid.

Observations of cavitation on the foil were made visually and photographically through the test-section viewing-window which was oriented opposite the concave face of the foil. Cavitation originating at the leading edge on the concave side could be fully observed and observations relative to the character and extent of the cavity were made. However, cavities on the convex side may originate at either the leading edge or in the vicinity of the point of maximum rise as determined by the orientation. The separate cavities from the convex side could only be observed for character and length when they extended beyond the trailing edge.

The observed cavitation is recorded herein by the series of high-speed photographs in Figs. 14 to 16, which serve to show the character of the cavities, and by the summary graph of Fig. 17, which shows the maximum length of the combined cavities. The lengths are as observed without correction for tunnel effects. The photographs were confined to tests at the lower angular settings and show only those portions of the cavities immediately adjacent to the foil.

As might be expected, the photographs show evidence of a variety of cavity forms including: (a) small, discrete, transient bubbles which in the mean appear essentially cloudy; (b) non-steady cavities in which the surging re-entrant jet causes the appearance to range from clear to cloudy; and (c) large cavities in which the forward portion is clear and steady, and the re-entrant jet processes are confined to a cloudy tail region. It should be noted that the cavities, in general, visually appear to have a stable average dimension, but high-speed still and motion pictures frequently disclose a definite pulsation from the re-entrant jet process. This pulsation could conceivably induce vibration in the foil in some applications, but there was no evidence of foil vibration in these tests. Because of the pulsing action, the photographs of Figs. 14 to 16 are not necessarily representative of the average cavity for the given test condition.

As a supplement to the foregoing pressure data, the graphic plottings were integrated to yield values for the lift coefficient, C_L, the drag coefficient, C_D, the ratio, C_L/C_D, and C_P, the distance from the leading edge to the center of the lift force expressed as a multiple of the foil chord length. These computed data are tabulated in Table II and the force relations are graphically summarized in the plottings of Figs. 18 and 19. It is to be noted that the computed values are based on the measured pressures from taps located only on the two faces of the foil. These make no account of the large positive unit pressures existing over the leading edge surfaces and the small skin friction effects. While it would have been desirable to determine the stagnation point and pressure distribution near the leading edge, the very limited dimensions in this region complicated proper tests. The error associated with this omission is deemed relatively unimportant with regard to the computed lift or to the computed drag values if they are used in comparison with the foil theory. However, for actual tests involving low α' and low σ, the cavity springing from the cylindrical leading edge may completely

Table II – Summary of Computed Data

C_{L_d} = 0.3 Edge A

α'	σ = 2.31				σ = 0.28				σ = 0.12				σ = 0.01			
	C_L	C_D	C_L/C_D	C_P	C_L	C_D	C_L/C_D	C_P	C_L	C_D	C_L/C_D	C_P	C_L	C_D	C_L/C_D	C_P
-4	.132	.031	4.26	1.38	-.078	.016	-4.80	-.01	-.065	.012	-5.38	.08	-.044	.008	-5.43	.10
-2	.332	.021	12.32	.73	.108	.022	4.94	1.13	-.037	.006	-6.71	.05				
0	.479	.019	25.22	.56	.265	.019	14.07	.64	-.006	.002	-3.15	1.14				
2	.641	.026	24.29	.48	.334	.021	16.20	.54	.196	.018	10.59	.62				
4	.842	.050	16.84	.41	.375	.033	11.42	.50	.302	.029	10.41	.52	.194	.023	8.49	.58
6	1.019	.084	12.16	.37	.409	.048	8.55	.48	.349	.042	8.39	.48				
8	1.133	.128	8.88	.35	.439	.064	6.85	.46	.384	.057	6.72	.46				
10	1.185	.173	6.85	.36	.466	.084	5.55	.45	.424	.076	5.61	.44	.365	.064	5.75	.43

C_{L_d} = 0.5 Edge A

α'	σ = 1.61				σ = 0.22				σ = 0.14			
	C_L	C_D	C_L/C_D	C_P	C_L	C_D	C_L/C_D	C_P	C_L	C_D	C_L/C_D	C_P
-4	.232	.083	2.81	.92	-.111	.016	-7.15	.06	-.158	.010	-15.76	.20
-2					-.072	.019	-3.81	-.10	-.124	.012	-10.47	.21
0	.646	.048	13.47	.57	.163	.042	3.93	.87	.009	.022	.41	4.58
2					.310	.044	7.02	.64	.286	.042	6.83	.65
4	1.070	.062	17.12	.49	.388	.050	7.75	.54	.401	.050	7.99	.54
6					.497	.065	7.61	.48	.477	.066	7.28	.50

C_{L_d} = 0.3

α'	Edge B						Edge C						Edge D		
	σ = 0.28			σ = 0.12			σ = 0.28			σ = 0.12			σ = 0.28		
	C_L	C_D	C_L/C_D	C_L	C_D	C_L/C_D	C_L	C_D	C_L/C_D	C_L	C_D	C_L/C_D	C_L	C_D	C_L/C_D
-2	.082	.025	3.34	.008	.010	.81	.125	.026	4.89	-.034	.010	-3.40	.034	.014	2.39
0	.220	.027	8.22	-.002	.010	-.20	.249	.022	11.17	-.019	.008	-2.51	.202	.024	8.24
2	.360	.023	15.77	.204	.023	8.78	.357	.035	10.26	.201	.017	11.78	.315	.026	12.20

envelope both surfaces of the foil as indicated in Figs. 11 and 15 and as previously observed by Martyrer [5]. The omission may be very serious as the lift and drag may be virtually zero when determined by the surface pressure values even though a significant drag exists on the leading edge. Dynamometer measurements of the drag would have served to clarify this omission but a dynamometer suitable to the purpose was not available at the time of the tests.

The C_P values listed in Table II have not been graphically summarized because they represent an incomplete concept of the moment conditions. They do, however, serve as a rough measure of the moment action and indicate the possibility of rapid changes and abnormalities when using negative angles under cavitating conditions.

The summary of measured force data given in Figs. 18 and 19 has been supplemented with additional comparative material from other sources.

Little data exist in the published literature for foils operating under severe cavitation, but certain of the data by Numachi and Murai [6], Numachi and Chida [7], and Walchner [8] are considered pertinent for moderate cavitation and are included in Figs. 18 and 19. The data have been selected for the non-cavitating case of $\sigma = 2.3$ and the moderately cavitating case $\sigma = 0.3$, and the angular values have been shifted 1.45 degrees to permit plotting in the α' scale of the foil with $C_{L_d} = 0.3$, as shown in Fig. 2. Foils were selected having about the same thickness ratio and the profiles of all foils are shown to scale in Fig. 20. It is to be noted that the data for Foil No. 4 were obtained with the foil in cascade, constituting a test environment which is less favorable to the performance than a single foil test, but more realistic.

As a further supplement to the test data in Fig. 18, curves are shown for the theoretical C_L values derived from the Tulin-Burkart relations for $\sigma = 0$.

Figures 18 and 19 clearly demonstrate the deficiencies of a cylindrical edge on the Tulin-Burkart foils when operated under conditions of low angle and severe cavitation. Tests were, therefore, conducted on the sharper alternate leading edges shown in Fig. 5. Since the tests were of a preliminary nature, they were confined to α' angular settings of -2, 0, and 2 degrees, and $\sigma = 0.28$ and 0.12. The measured pressure distribution data for these

edges are shown in Figs. 21 to 23 and the force integrations computed from the pressure distribution curves have been listed in Table II and graphically summarized in Fig. 24.

VI. DISCUSSION OF FINDINGS

The foil cavitation tests described herein are an initial phase of a continuing program for the performance improvement of foils operating under conditions of extreme cavitation. This report is an interim description of the studies and, as such, is not conclusive in design findings. There are, however, a number of useful observations which may be cited at this phase of the study.

The experimental study has served to clarify the prime importance of the leading edge configuration under low σ conditions of flow. The thin cylindrical leading edges, which were tested as a fabricating compromise with the thin edge requirements of the theory, did not yield high performance characteristics at small α' and σ, and it appears essential that thin, sharp edges be employed if such performance is to be achieved.

Sharp edges are also essential to present methods of theoretical foil analysis and the objective of establishing a practical design theory will be promoted by adherence to sharp edges in forthcoming tests. It must be recognized that edges which possess the sharpness necessary to the lowest drag performance will be readily susceptible to mechanical damage and structural failure. For this reason, compromise edge forms of lower performance, but greater durability may eventually be sought.

The solution of the relations established by Tulin and Burkart is dependent on the simplifying assumption that $\sigma = 0$. This condition cannot be achieved in either test or application installations; hence, full correlation of the present relations is not to be expected. An appropriate eventual theoretical development should, however, permit evaluations at σ other than zero, as does the theory of Wu [9] for circular arcs. Comparison of the Tulin-Burkart foil data ($\sigma = 0.3$) with the circular segment foil of Walchner in Fig. 19 shows a considerable similarity of performance when superimposed by a suitable shift in defined angle of attack. There is reason to believe that the experimentally tested Tulin-Burkart foil would show a superior performance if provided with the same edge sharpness as the Walchner foil. (There is

some reason to question the validity of the Walchner data on the basis of other water tunnel experience at the St. Anthony Falls Laboratory, for it is difficult to understand how the early Gottingen tunnel employed by Walchner could operate at $\sigma = 0.0$ and 0.1 as indicated when other modern closed-jet tunnels are faced with serious operating difficulties at considerably higher values. A question also arises relative to the short length of the Walchner cavities as compared with the St. Anthony Falls Laboratory data shown in Fig. 17.)

Limited tests have been conducted to determine the influence of the contact viewing-window on the pressure field of the free jet. These tests are incomplete but indicate substantial secondary effects and the need for a comprehensive study of blockage and interference corrections for the cavitating flow.

The tests described herein do not include pressure or force evaluations for the cylindrical leading edge of the foils, but some insight into the magnitude of the drag effect may be obtained from the related cylinder cavitation data of Martyrer [5]. In those tests the pertinent C_D value (based on projected frontal area) for a cavitating cylinder ranged from 0.5 to 1.1. If these limits are applied to the St. Anthony Falls Laboratory foil with an edge cylinder of 0.035-in. diameter and chord of 2.5 in., the equivalent conventional foil C_D value (based on foil area) would range from 0.007 to 0.015. While these are low absolute values they are of significant magnitude when compared to the measured C_L and C_D values listed in Table II for low α' and low σ.

It was originally anticipated that at least one of the leading edge modifications of Fig. 5 would show a significant performance improvement over the original edge cylinder. The rather surprising results shown in Fig. 24 are unexplained but serve to further emphasize the importance of leading edge studies for thin hydrofoils.

The thin airfoil theory and flat plate approximation basic to the Tulin-Burkart relations includes the lift expression $C_L = \frac{\pi \alpha'}{2} + C_{L_d}$. For purposes of comparison plots of this expression have been included in Fig. 18. A comparison between the computed values and the test data for lowest σ indicates a good general agreement in slope, but a marked difference in absolute magnitudes. The difference has not been resolved. Basic relations for the

case of non-cavitating flow yield a similar lift curve (not shown) having a slope of 2π . It is noteworthy that the non-cavitating tests of the Tulin-Burkart foils, as shown in Fig. 18, roughly approximate this slope. The theoretical angle of zero lift is, however, again very different from that of the test data.

The tests indicate that the pressure within the foil cavity is greater than vapor pressure by an amount significant to the evaluation of the cavitation parameter σ . The influence on σ decreases as the magnitude of σ decreases.

VII. FUTURE STUDIES

The studies described have served to establish certain techniques for measuring the characteristics of supercavitating hydrofoils and have disclosed certain deficiencies of the foils tested. In light of these studies, the following items are to be given consideration in the continuing phases of the study:

A. Correlation of foil theory with foil performance in a free-jet tunnel is not yet established for extreme cavitation conditions. Hence, it appears advisable to test certain of the elementary flat plates, circular arcs, and circular segments along with proposed high-performance foil designs.

B. Comparative performance tests can be conducted more readily by measuring foil forces rather than by pressure distributions. It is proposed to assemble a two-component force dynamometer for this purpose and parallel such measurements with only limited pressure studies.

C. Limited tests intended to clarify the influence of the free-jet boundary and viewing-window on the test data have indicated a complexity requiring further tests and study.

D. Little information exists on the configuration of the free surface of the cavity accompanying the performance of a given foil. For purposes of establishing the related theory, and the influence of leading edge form, it is desirable that the present cavity length measurements be supplemented by more refined measurements of cavity extent and shape.

E. In studying new high-performance foil designs, considerable thought should be given to the leading edge shape, and tests should seek to establish the limiting flow and structural instabilities of selected shapes.

LIST OF REFERENCES

[1] Tulin, M. P. and Burkart, M. P. Linearized Theory for Flows About Lifting Foils At Zero Cavitation Number. Report C-638, David Taylor Model Basin, February 1955. Confidential.

[2] Christopherson, C. D. Description of a Ten-Inch Free-Jet Water Tunnel. University of Minnesota, St. Anthony Falls Hydraulic Laboratory, Project Report No. 35, January 1953.

[3] Olson, R. M. Cavitation Testing in Water Tunnels. University of Minnesota, St. Anthony Falls Hydraulic Laboratory, Project Report No. 42, December 1954.

[4] Self, M. W. and Ripken, J. F. Steady State Cavity Studies in a Free-Jet Water Tunnel. University of Minnesota, St. Anthony Falls Hydraulic Laboratory, Project Report No. 47, July 1955.

[5] Martyrer, V. E. "Kraftmessungen an Widerstandskorpern und Flugelprofilen im Wasserstrom bet Kavitation." Hydromechanische Probleme Des Schiffsantriebs, edited by G. Kempf and E. Foerster, Hamburg, Germany 1932. Pp. 268-286.

[6] Numachi, F. and Murai, H. "Cavitation Tests on Hydrofoil Profiles Suitable for Arrangement in Cascade." Reports of the Institute of High Speed Mechanics, Vol. 2, 1952, Tohoku University, pp. 1-19.

[7] Numachi, F. and Chida, I. "Effect of Static Pressure Differences on the Cavitation Characteristics of Hydrofoil Profile." Reports of the Institute of High Speed Mechanics, Vol. 5, 1955, Tohoku University, pp. 37-47.

[8] Walchner, O. "Profilmessungen Bei Kavitation." Hydromechanische Probleme des Schiffsantriebs, edited by G. Kempf and E. Foerster, Hamburg, Germany 1932. Pp. 256-267. (Translated and published as National Advisory Committee for Aeronautics, Technical Memorandum No. 1060.

[9] Wu, T. Y. A Free Streamline Theory for Two-Dimensional Fully Cavitated Hydrofoils, Report No. 21-17, Hydrodynamics Laboratory, California Institute of Technology, July 1955.

FIGURES
(1 through 24)

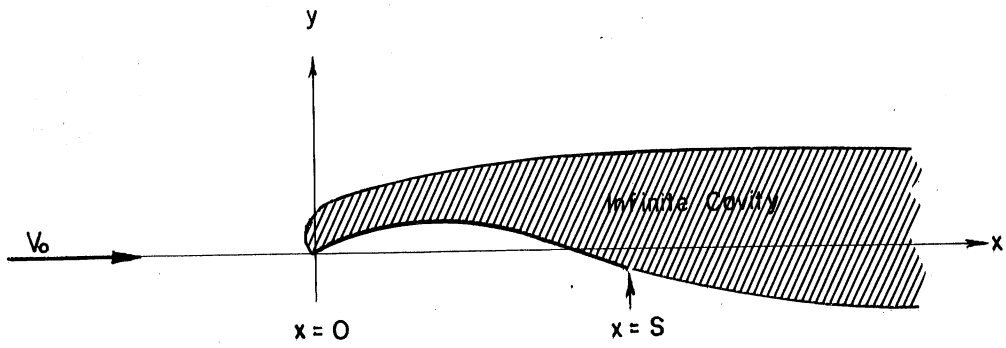

Fig. 1 – Schematic Orientation of the Supercavitating Hydrofoil at $\sigma = 0$

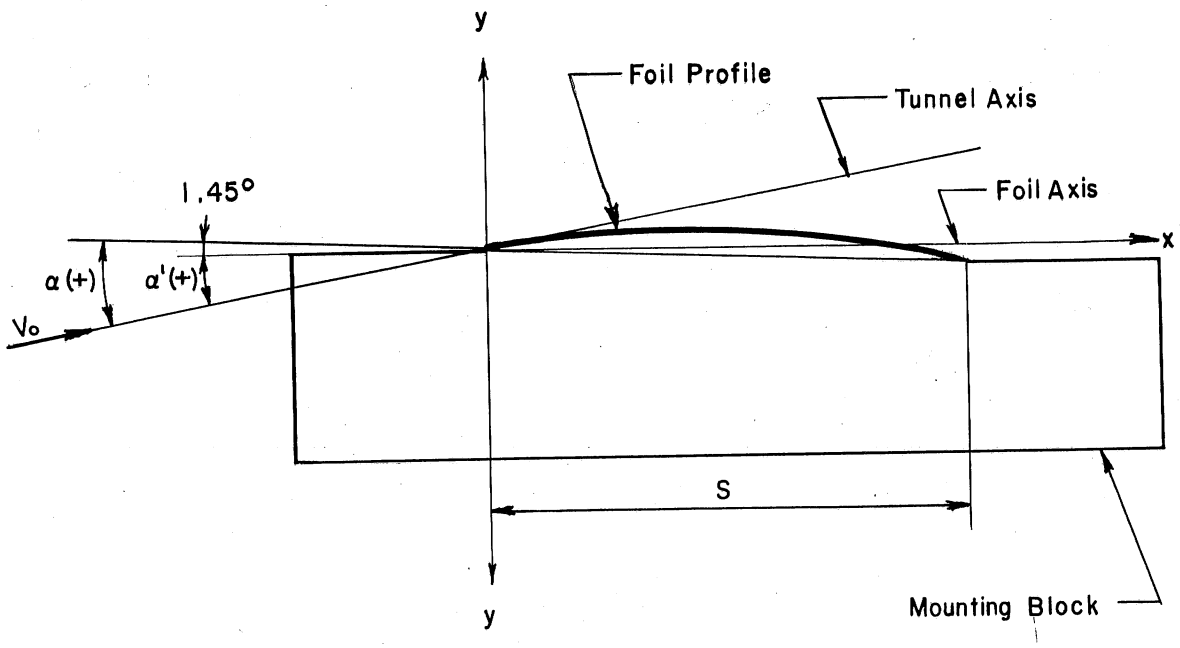

Fig. 2 – Full Scale Profile and Orientation on Mounting Block for Foil with $C_{L_d} = 0.3$ and S = 2.5 inches

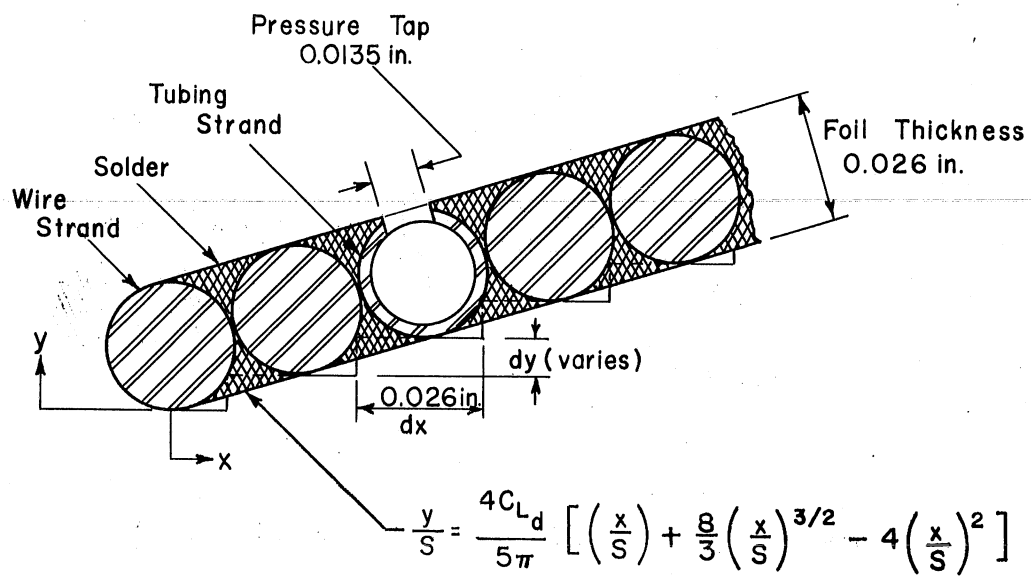

(a) Foil with $C_{L_d} = 0.5$, $S = 2.5$ in.

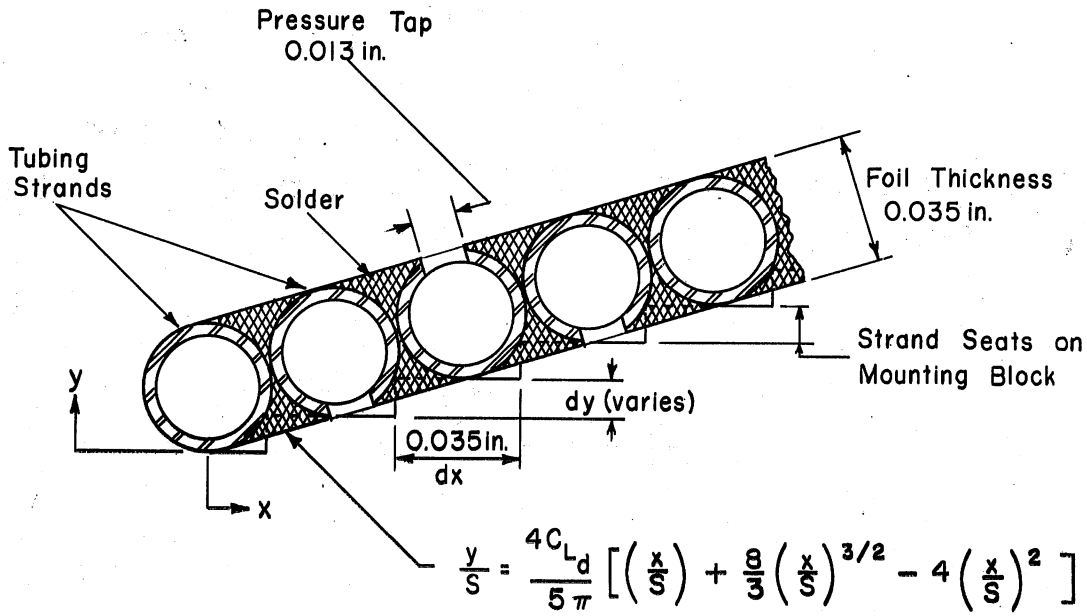

(b) Foil with $C_{L_d} = 0.3$, $S = 2.5$ in.

Fig. 3 – Fabricating Details for the Test Foils

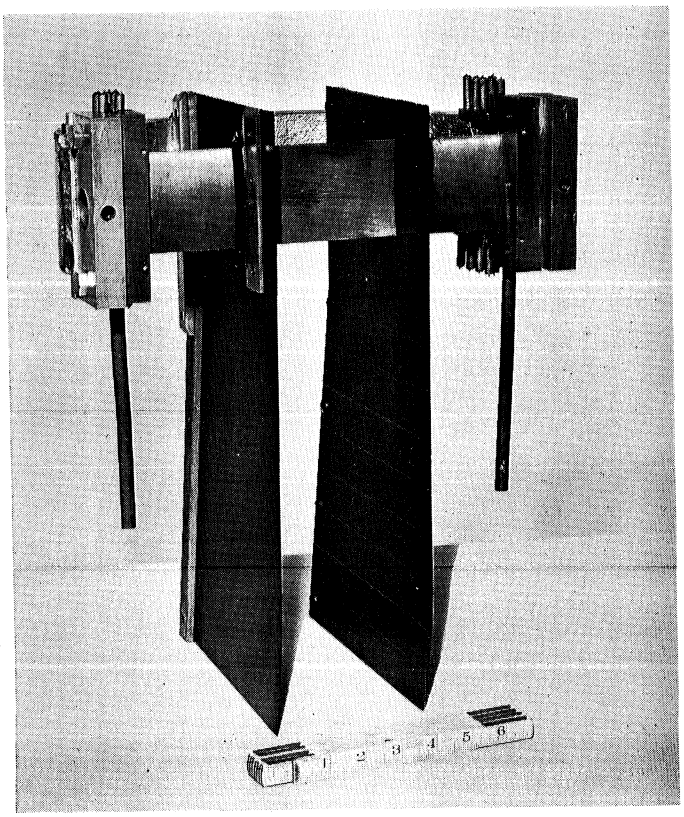

a. Viewed from Concave Face

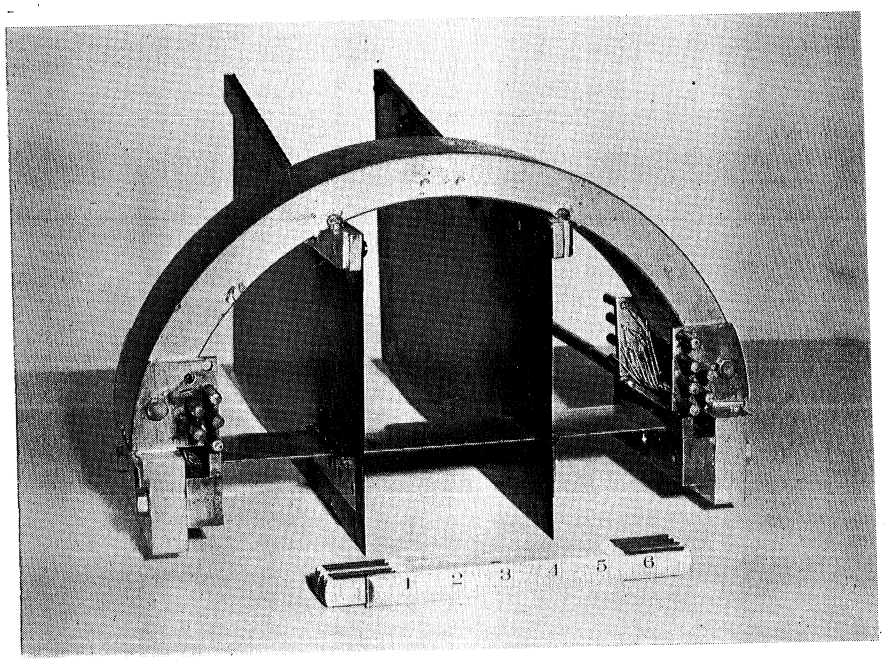

b. Viewed from Upstream

Fig. 4 - Bench Assembly of a Test Hydrofoil (C_{L_d} = 0.3)

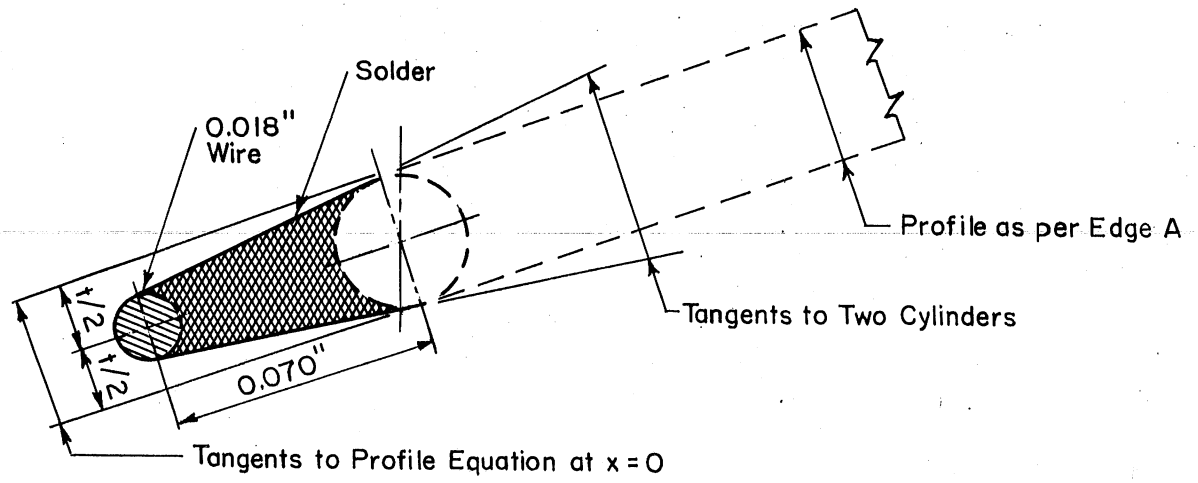

Leading Edge B

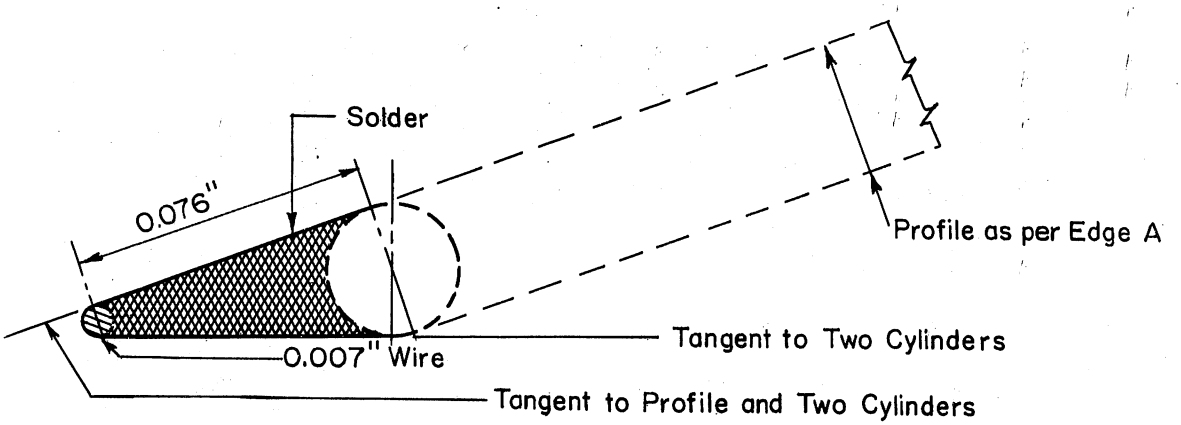

Leading Edge C

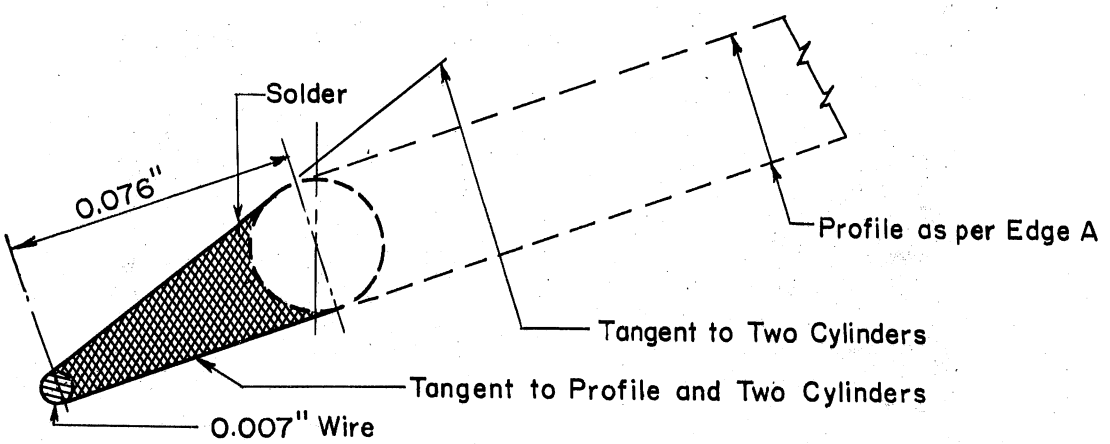

Leading Edge D

Fig. 5 – Alternate Forms of Leading Edges

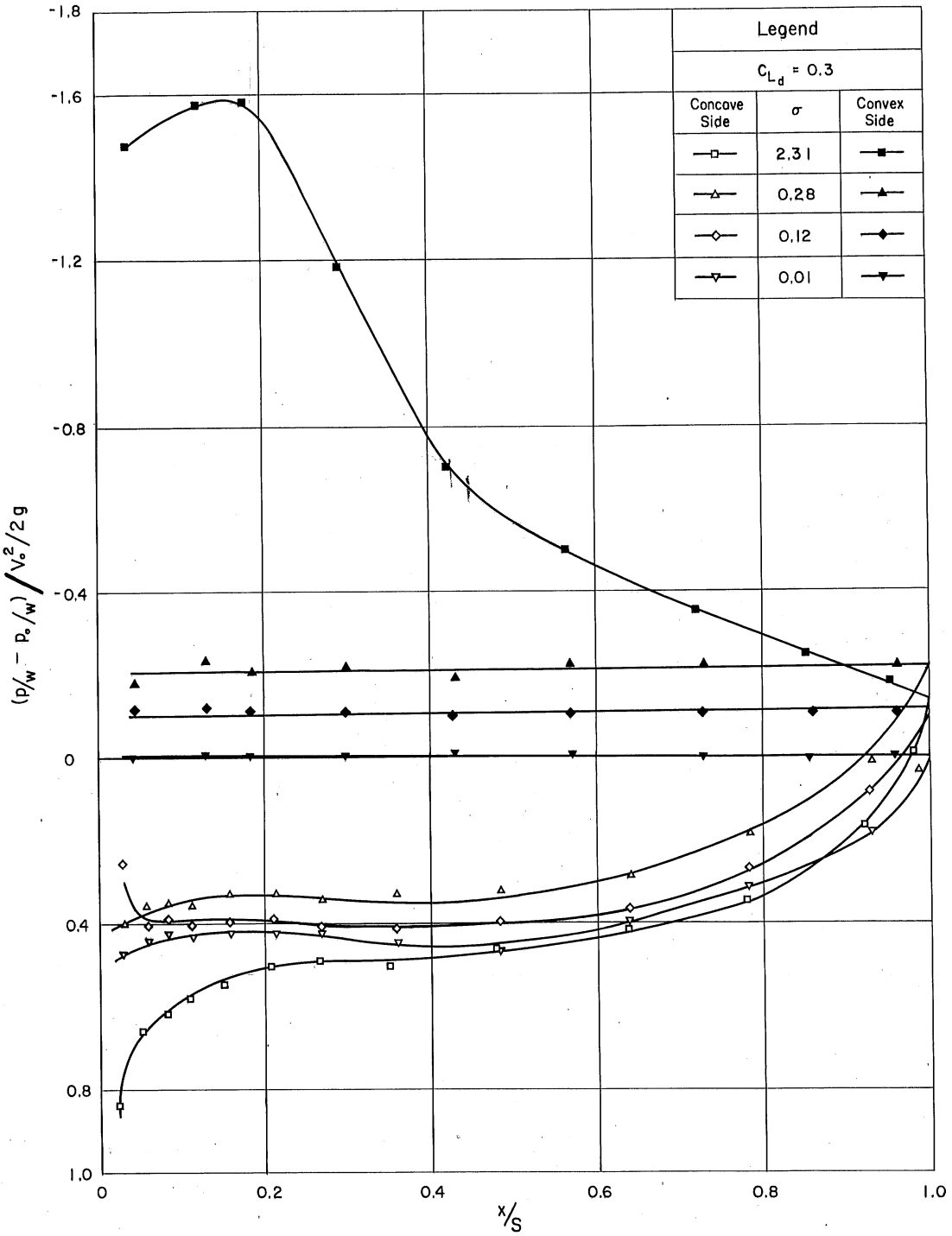

Fig. 6 - Measured Pressure Distributions $\alpha' = 10$, Edge Type A

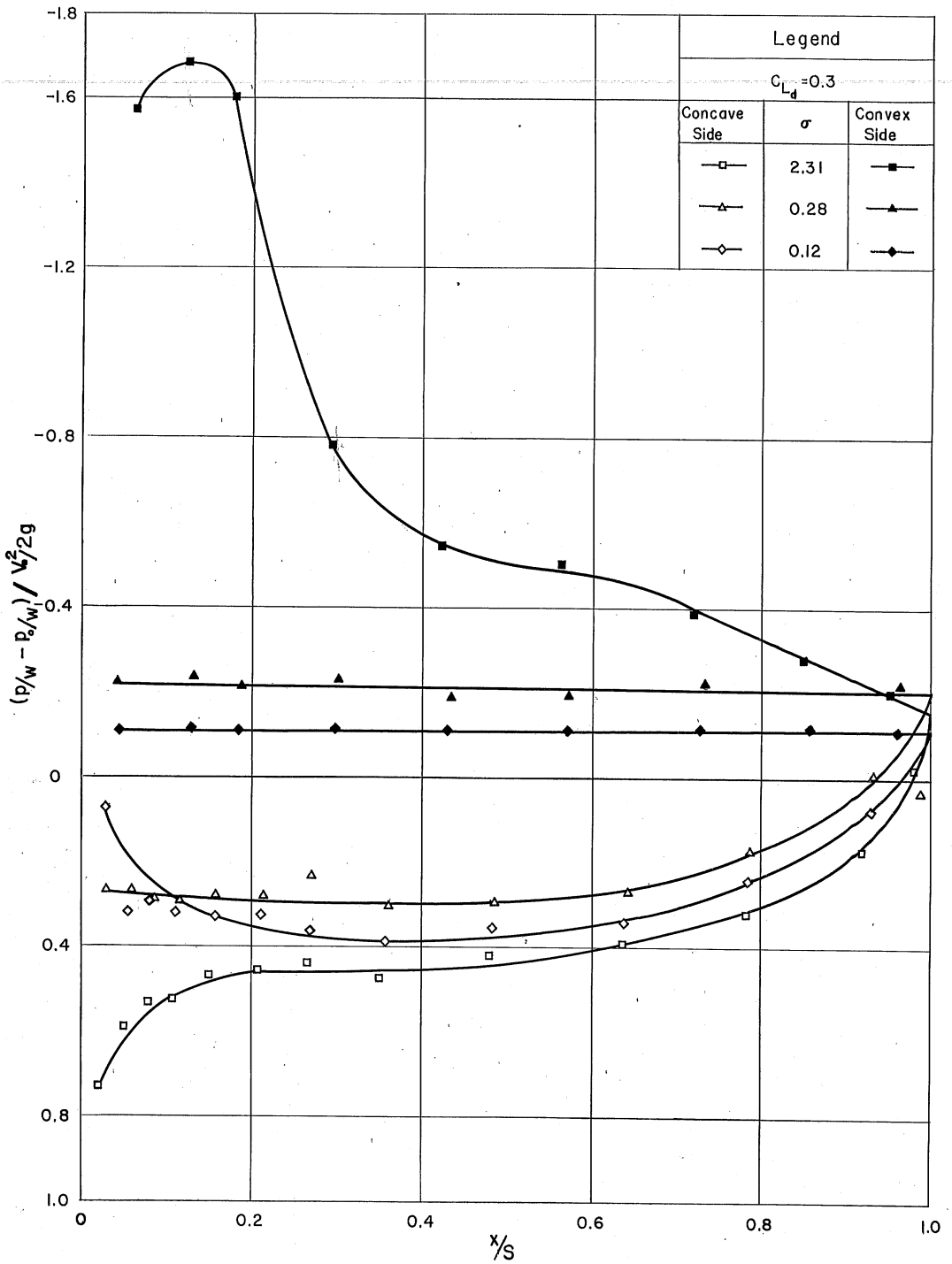

Fig. 7 - Measured Pressure Distributions α^1 = 8, Edge Type A

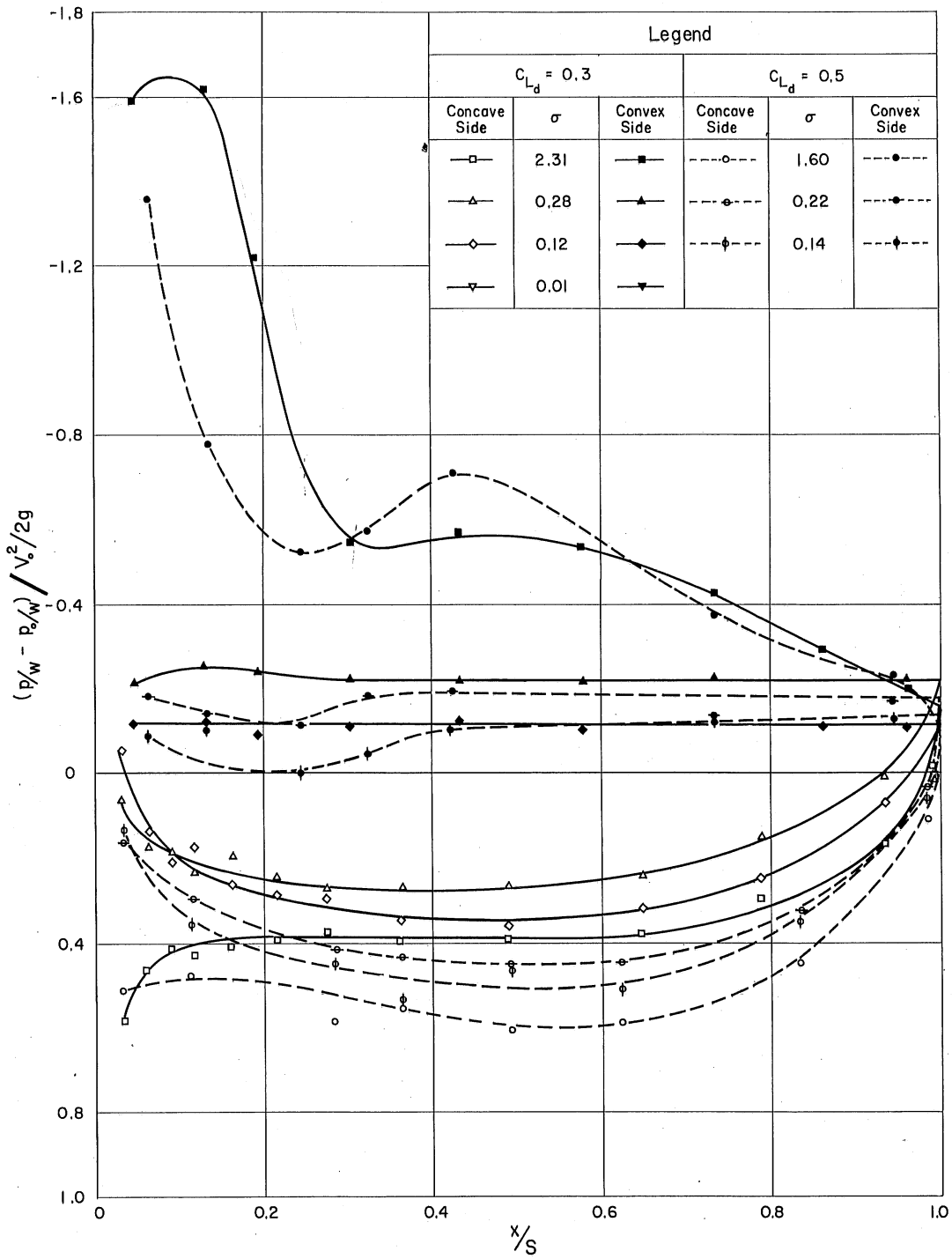

Fig. 8 – Measured Pressure Distributions $\alpha' = 6$, Edge Type A

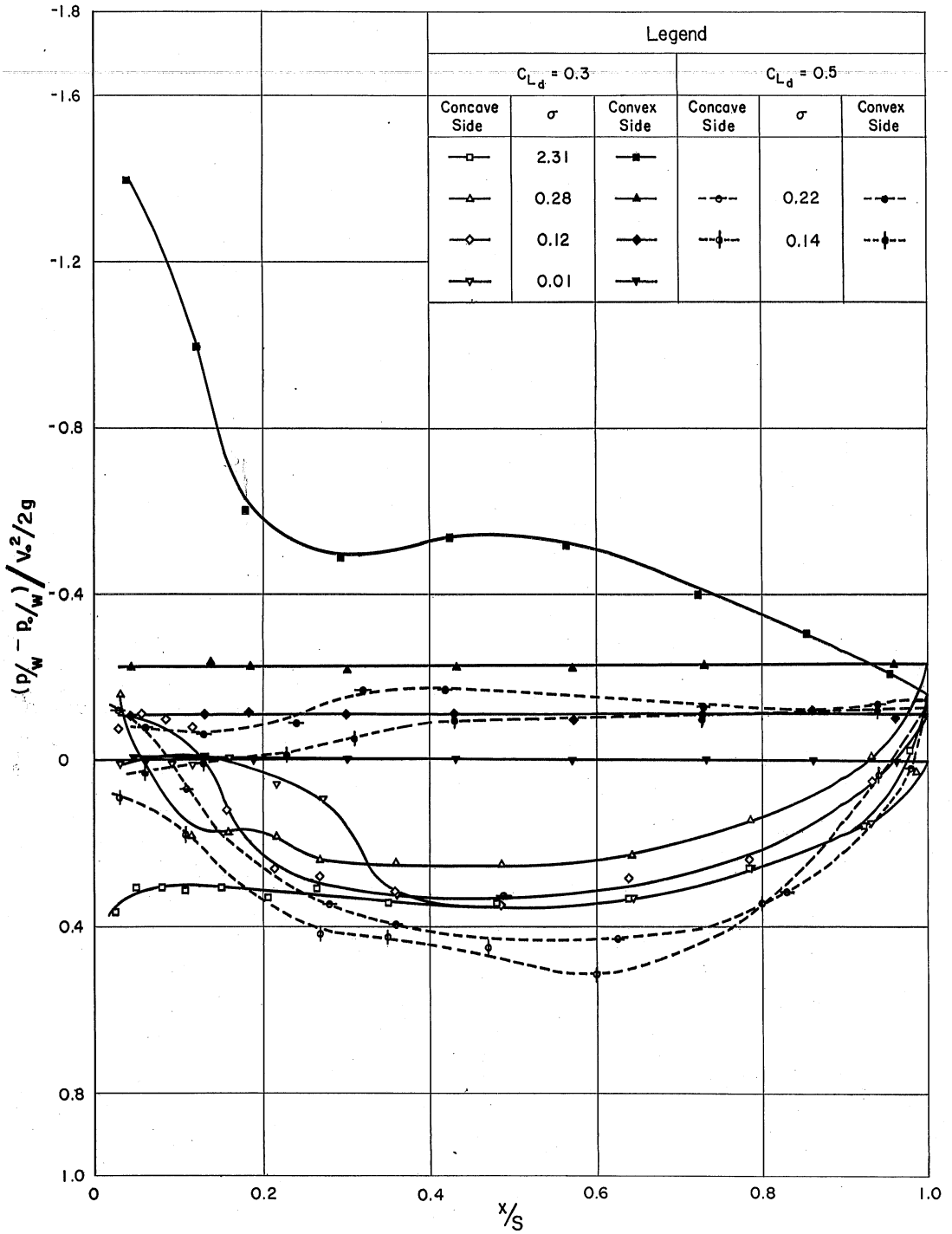

Fig. 9 – Measured Pressure Distributions $\alpha' = 4$, Edge Type A

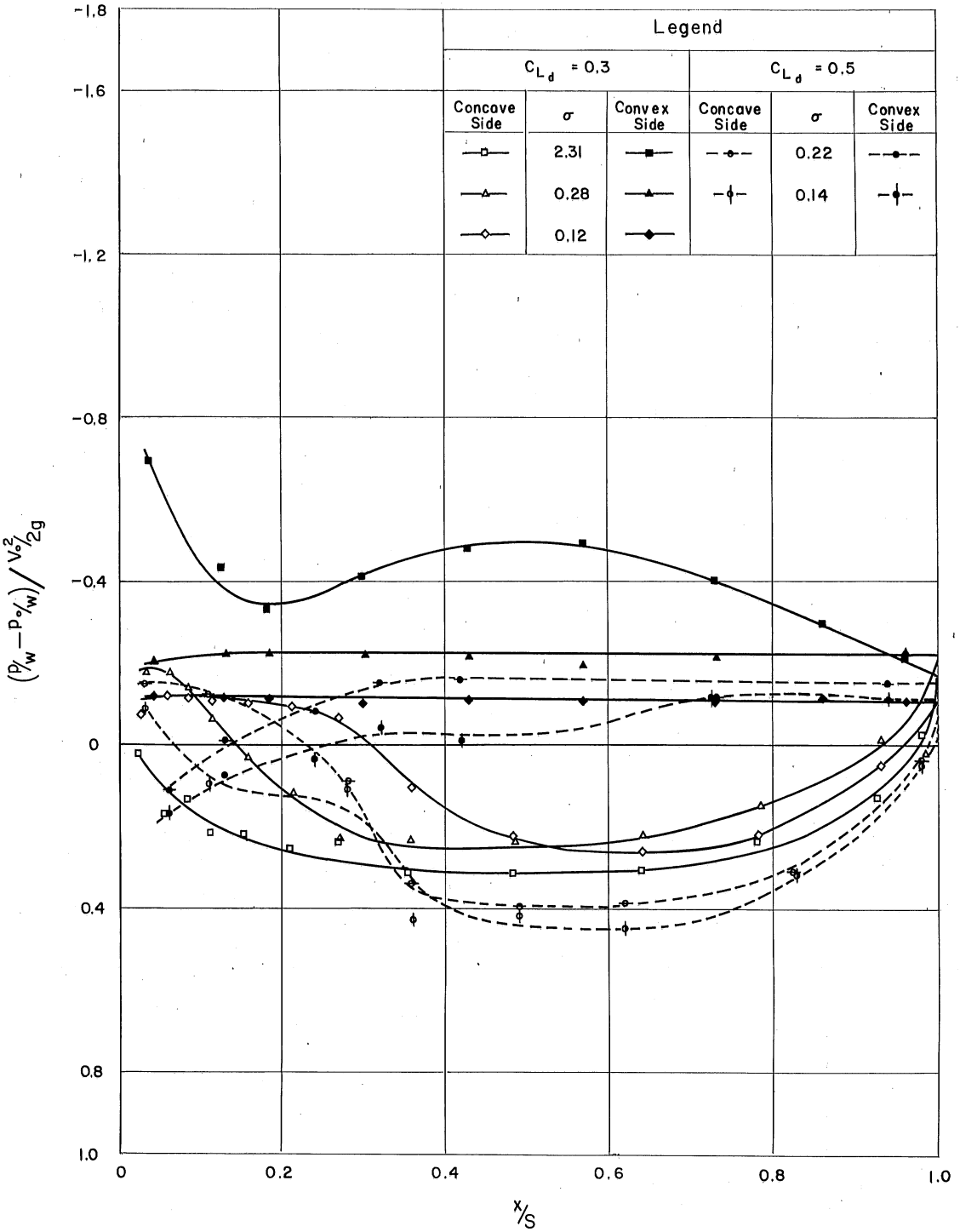

Fig. 10 – Measured Pressure Distributions $\alpha' = 2$, Edge Type A

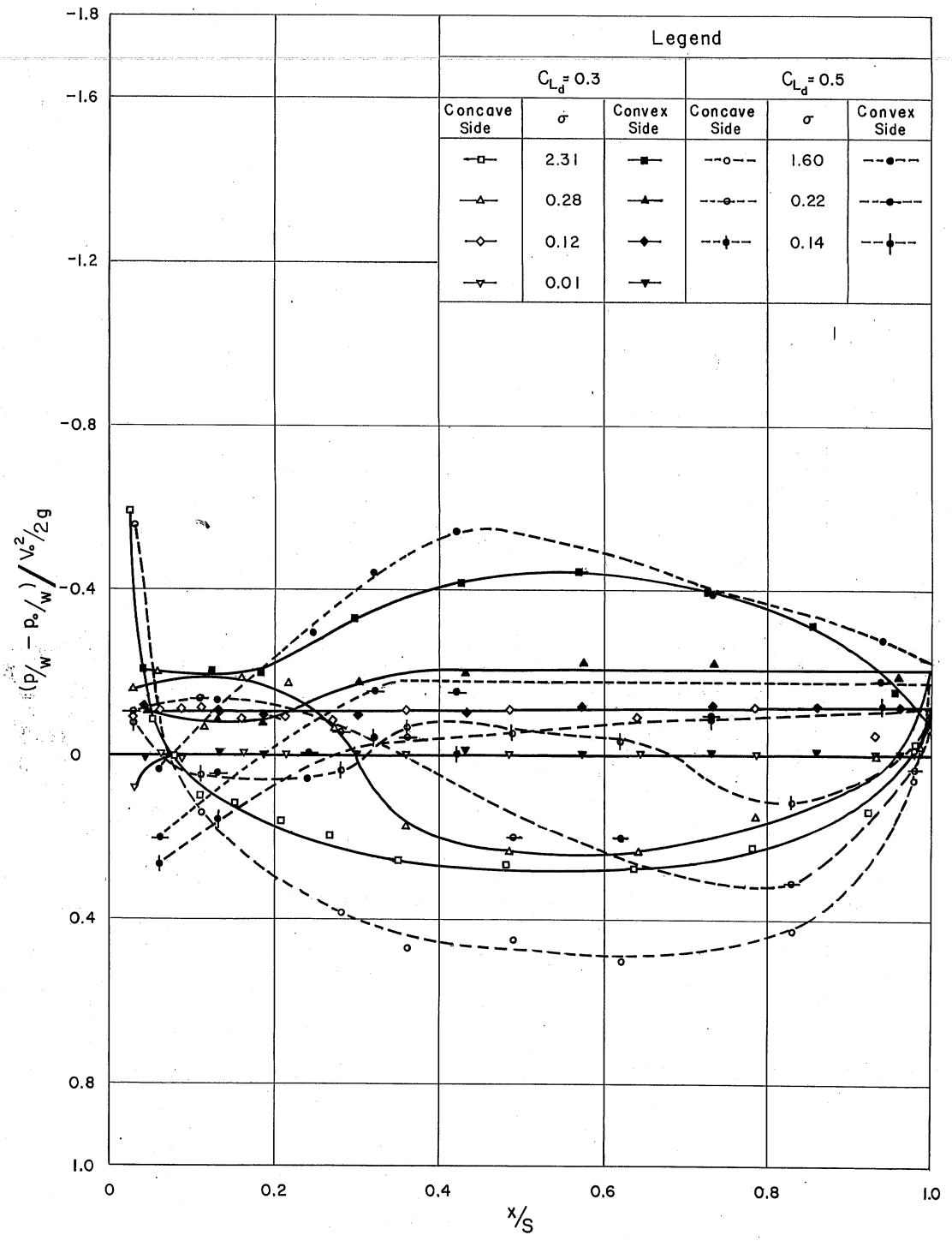

Fig. 11 – Measured Pressure Distributions $\alpha' = 0$, Edge Type A

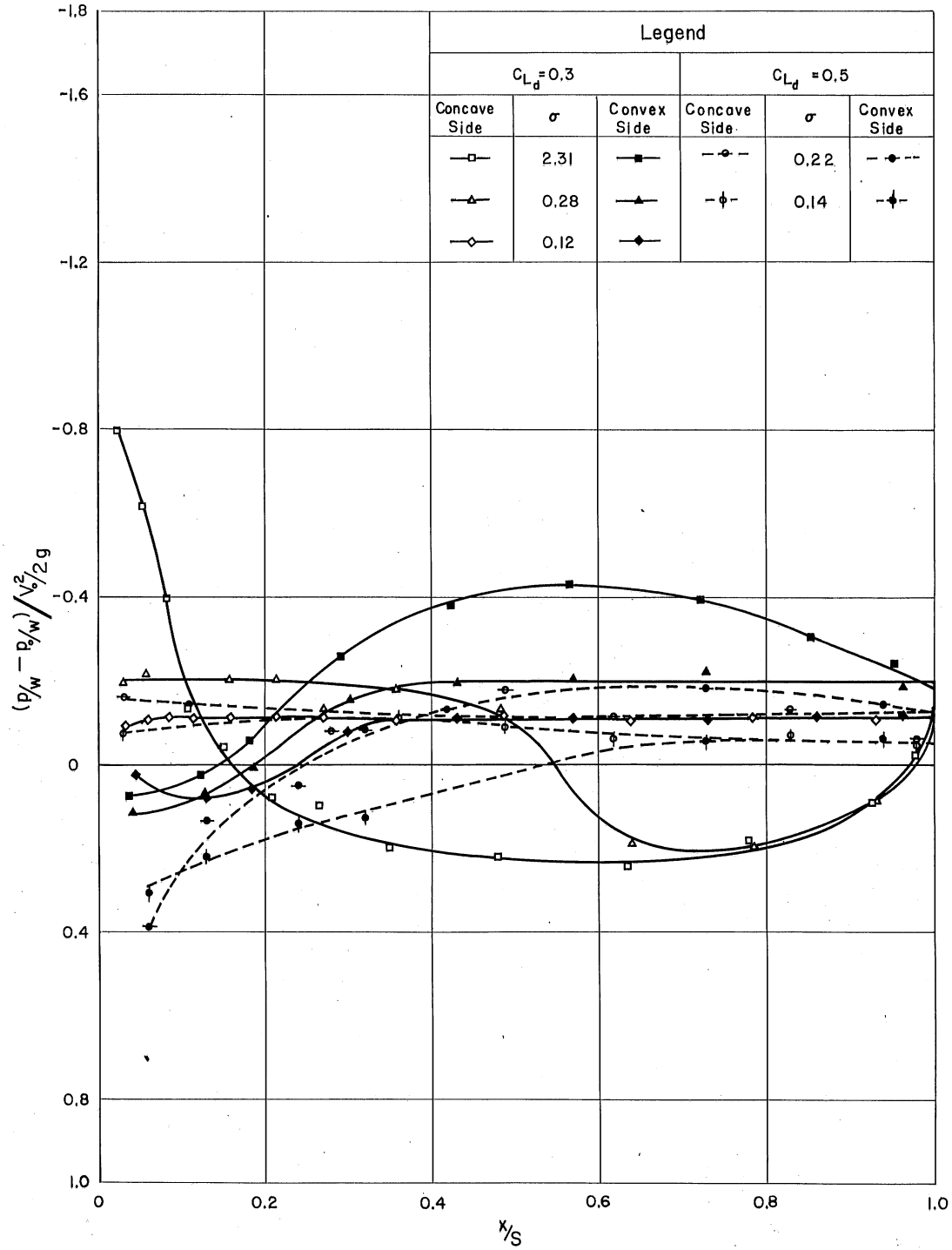

Fig. 12 – Measured Pressure Distributions $\alpha' = -2$, Edge Type A

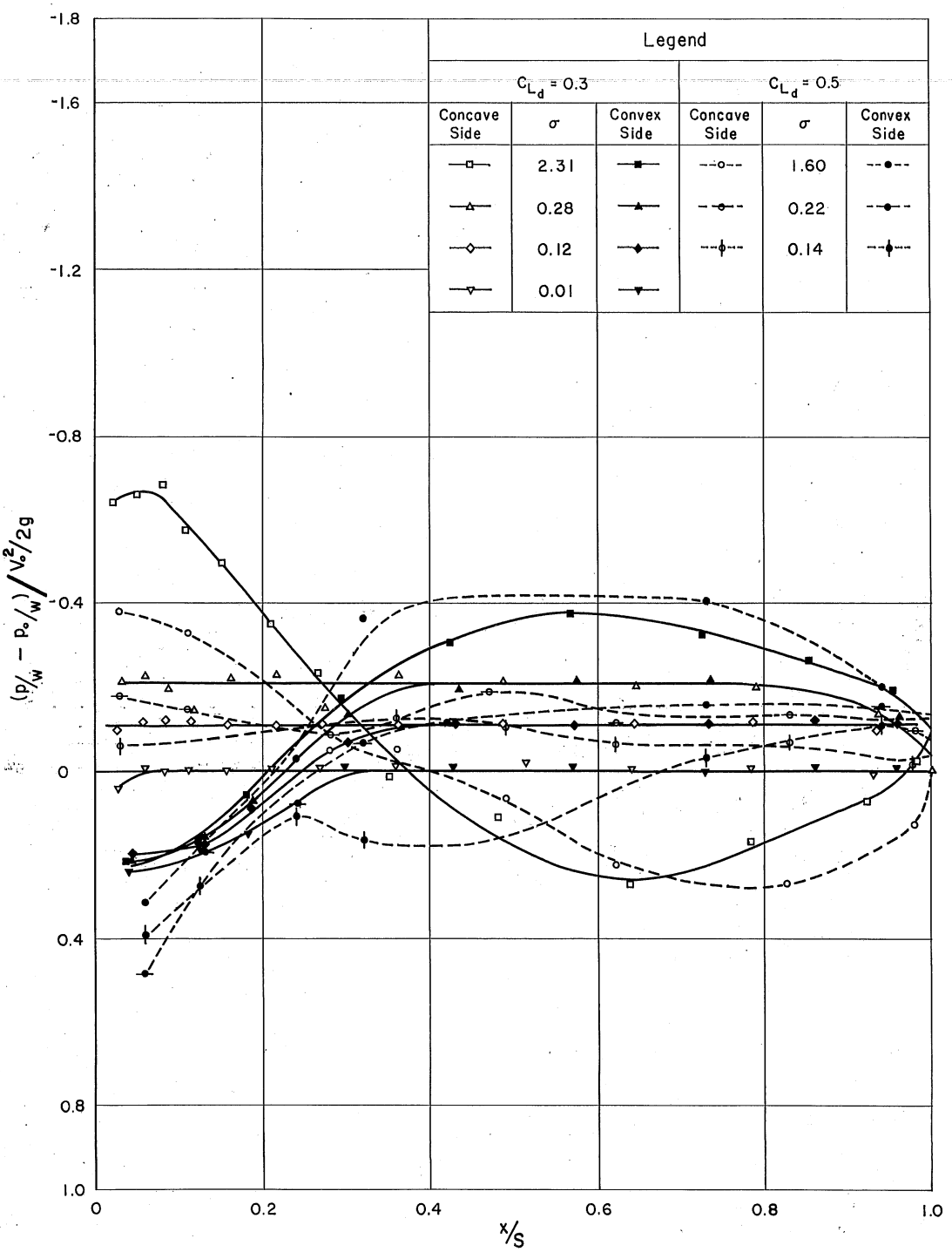

Fig. 13 - Measured Pressure Distributions $\alpha' = -4$, Edge Type A

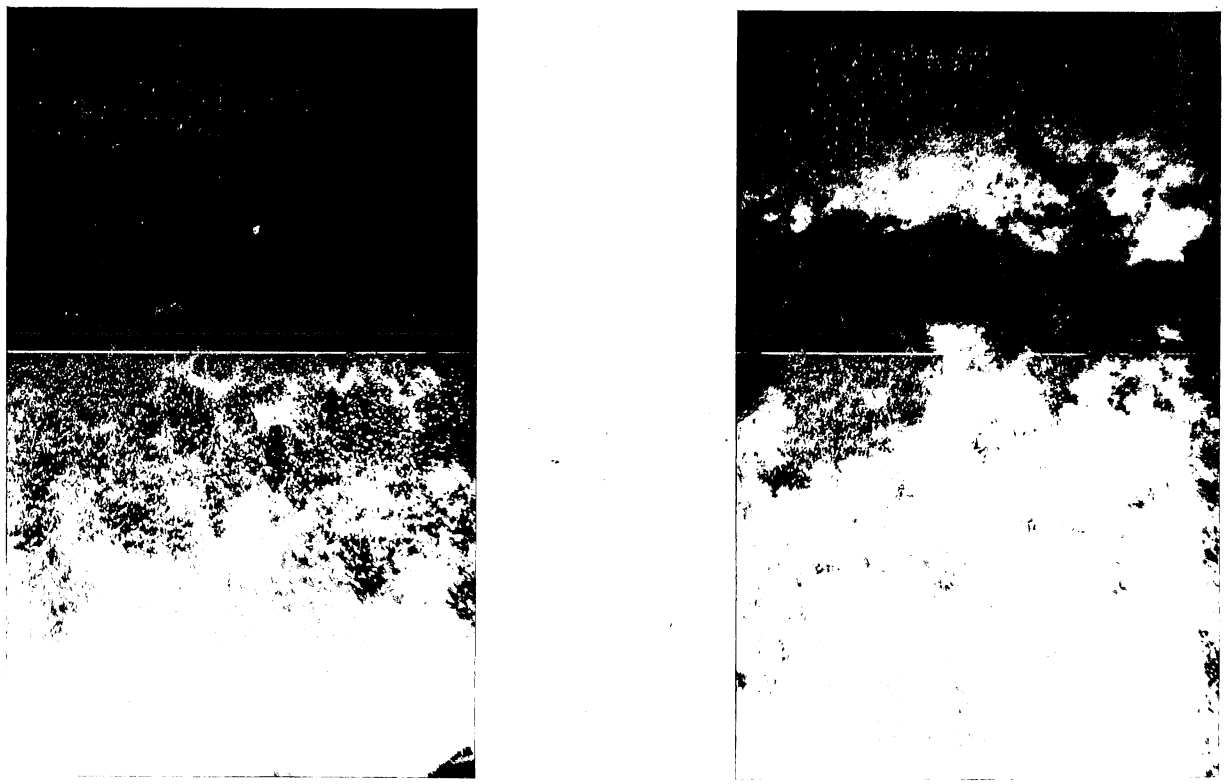

σ = 0.19 σ = 0.07

Fig. 14 - Photographic Cavity Studies, C_{L_d} = 0.3, Edge A, α' = 2

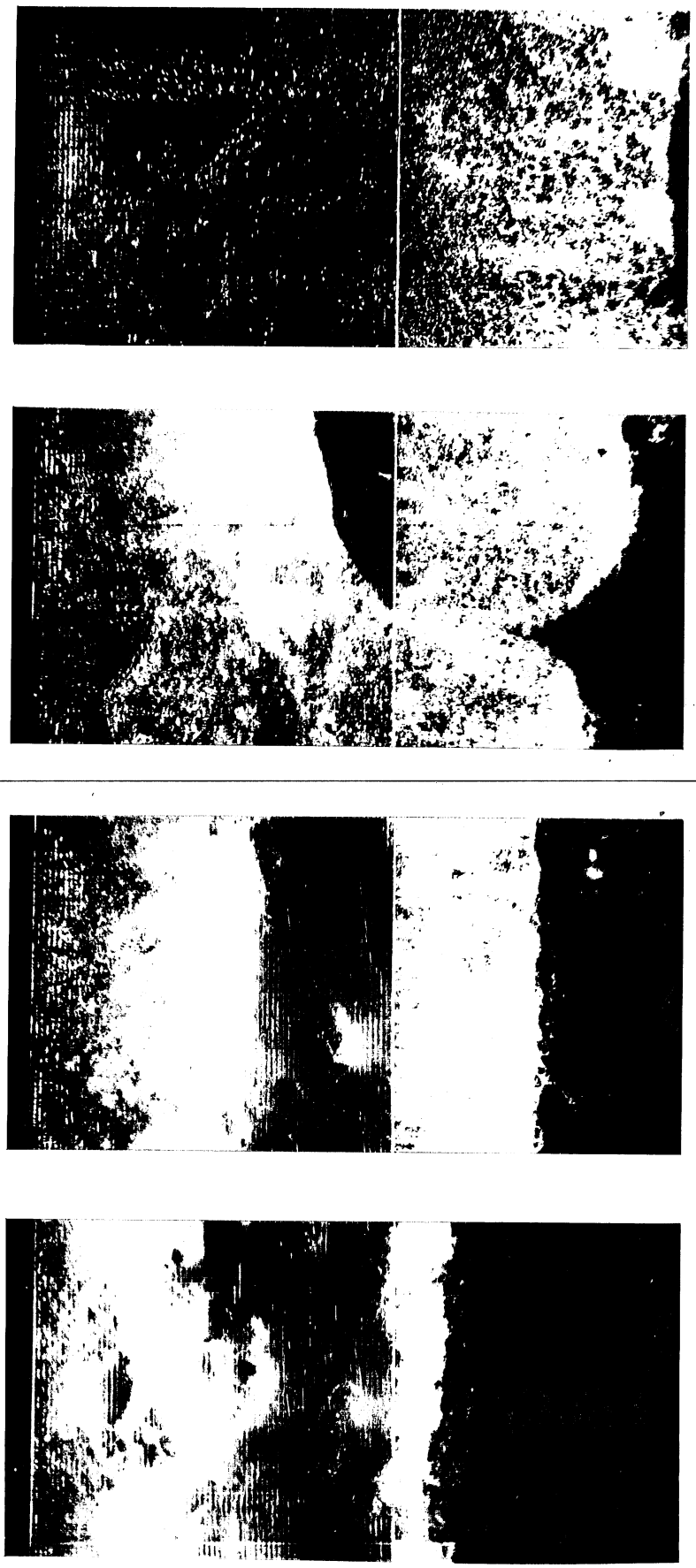

Fig. 15 – Photographic Cavity Studies, $C_{L_d} \cong 0.3$, Edge A, $\alpha' = 0$

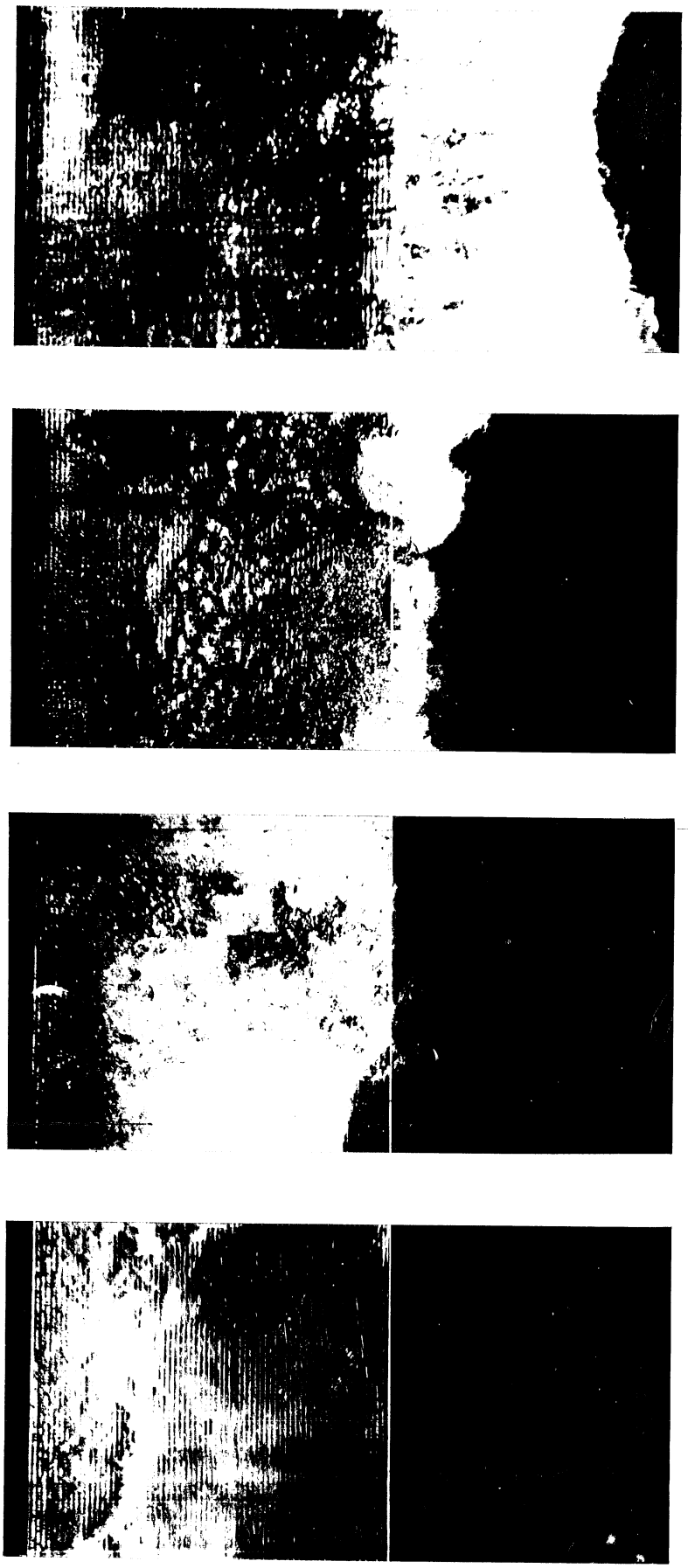

σ = 0.15

σ = 0.19

σ = 0.20

σ = 0.49

Fig. 16 – Photographic Cavity Studies, $C_{L_d} = 0.3$, Edge A, $\alpha' = -2$

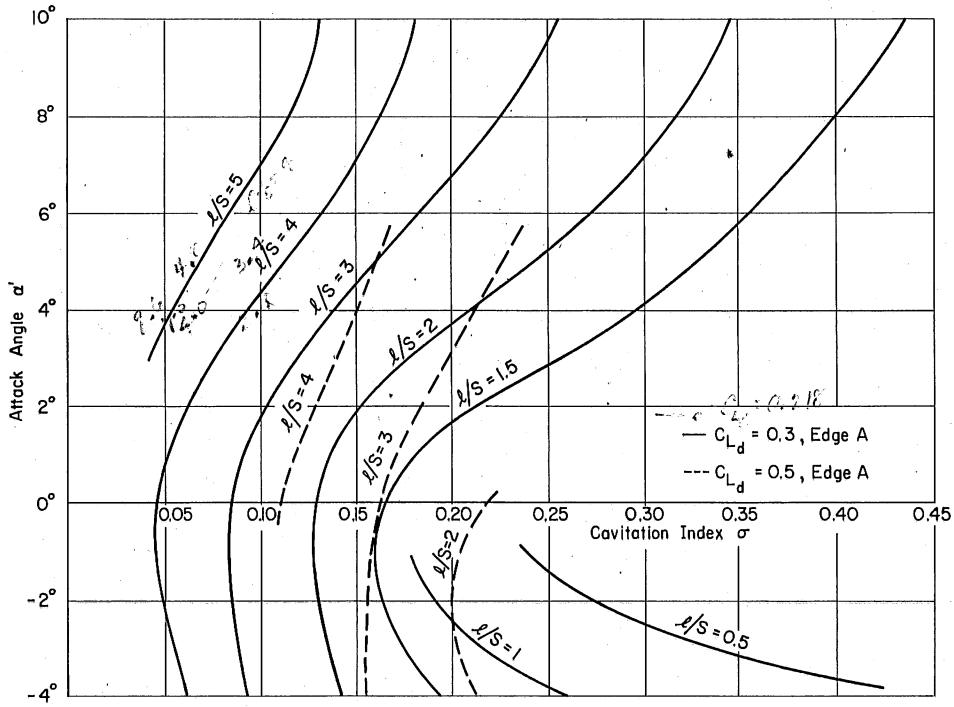

Fig. 17 – Approximate Maximum Length of Foil Cavities Under Various Testing Conditions

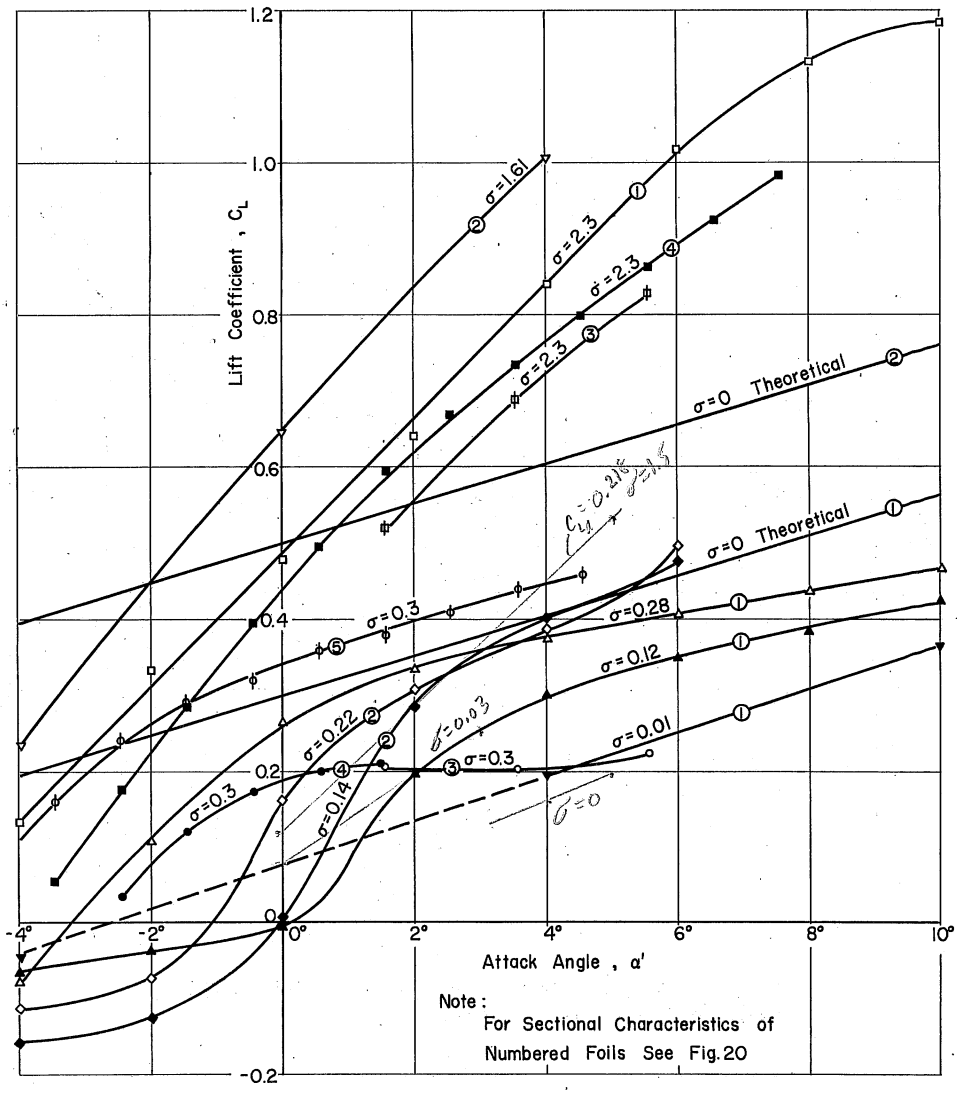

Fig. 18 – Comparative Lift Data for Various Foil Sections and Test Conditions

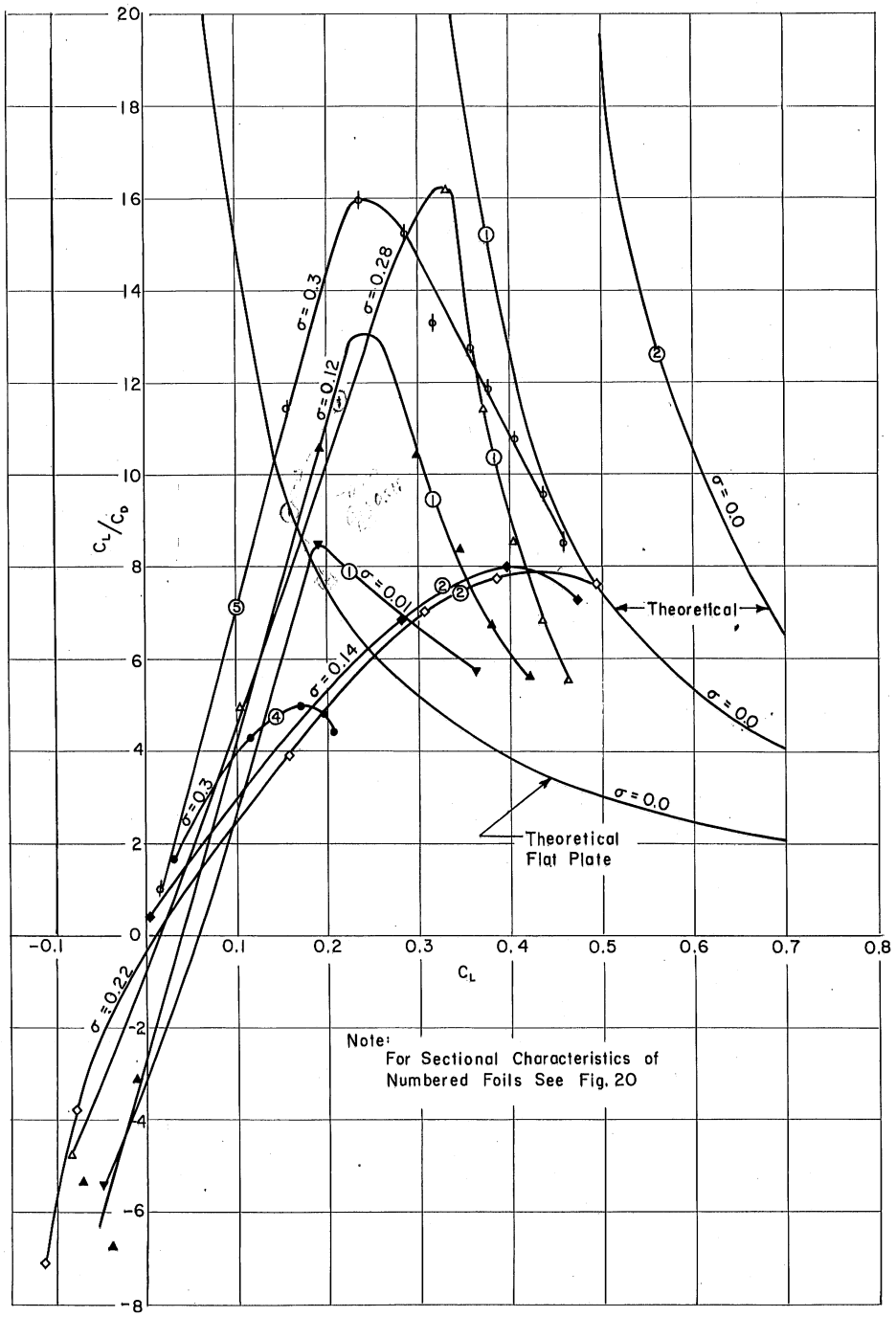

Fig. 19 - Comparative C_L/C_D Ratios for Various Foil Sections and Test Conditions

Foil No.	Shape	Foil Source	Data Source
1	0.034S / 0.025S	Tulin - Burkart $C_{L_d} = 0.3$	SAF Tests
2	0.057S / 0.042S	Tulin - Burkart $C_{L_d} = 0.5$	SAF Tests
3	0.07S	Numachi 0_7^4	Numachi Tests
4	0.08S	Clark Y.8	Numachi Tests
5	0.0735S	Circular Segment	Walchner Tests

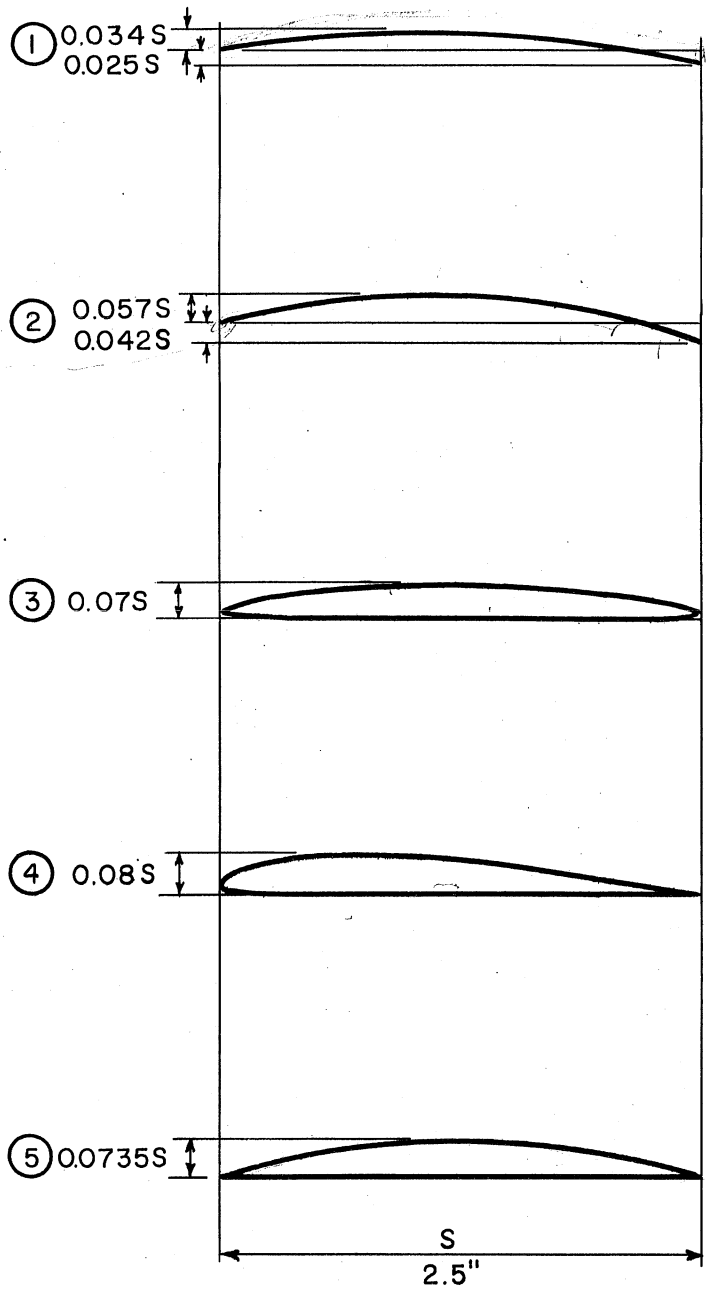

Fig. 20 – Profile Sections of the Foils Treated in Figs. 18 and 19

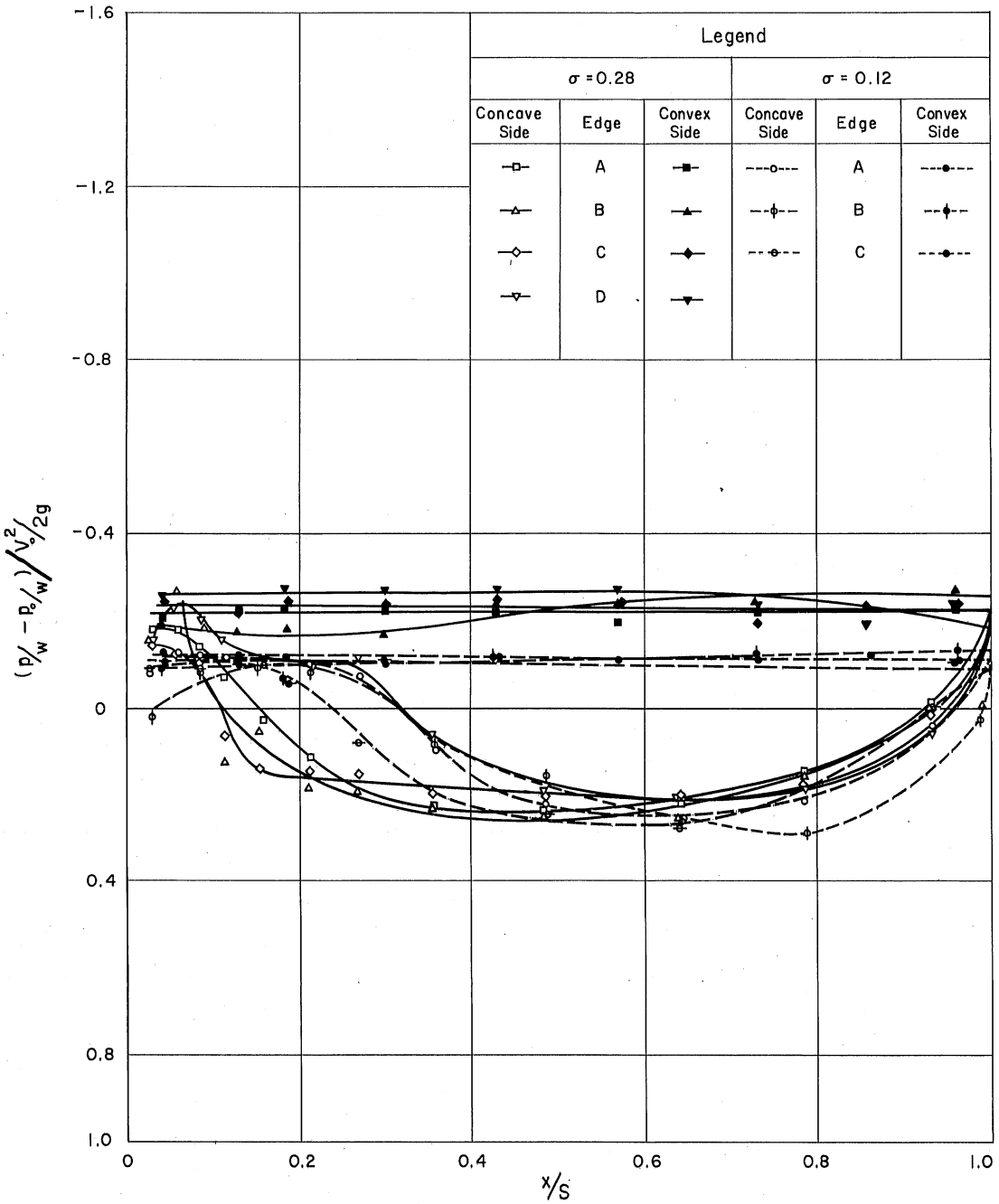

Fig. 21 - Measured Pressure Distributions, Alternate Edge Types, $\alpha' = -2$

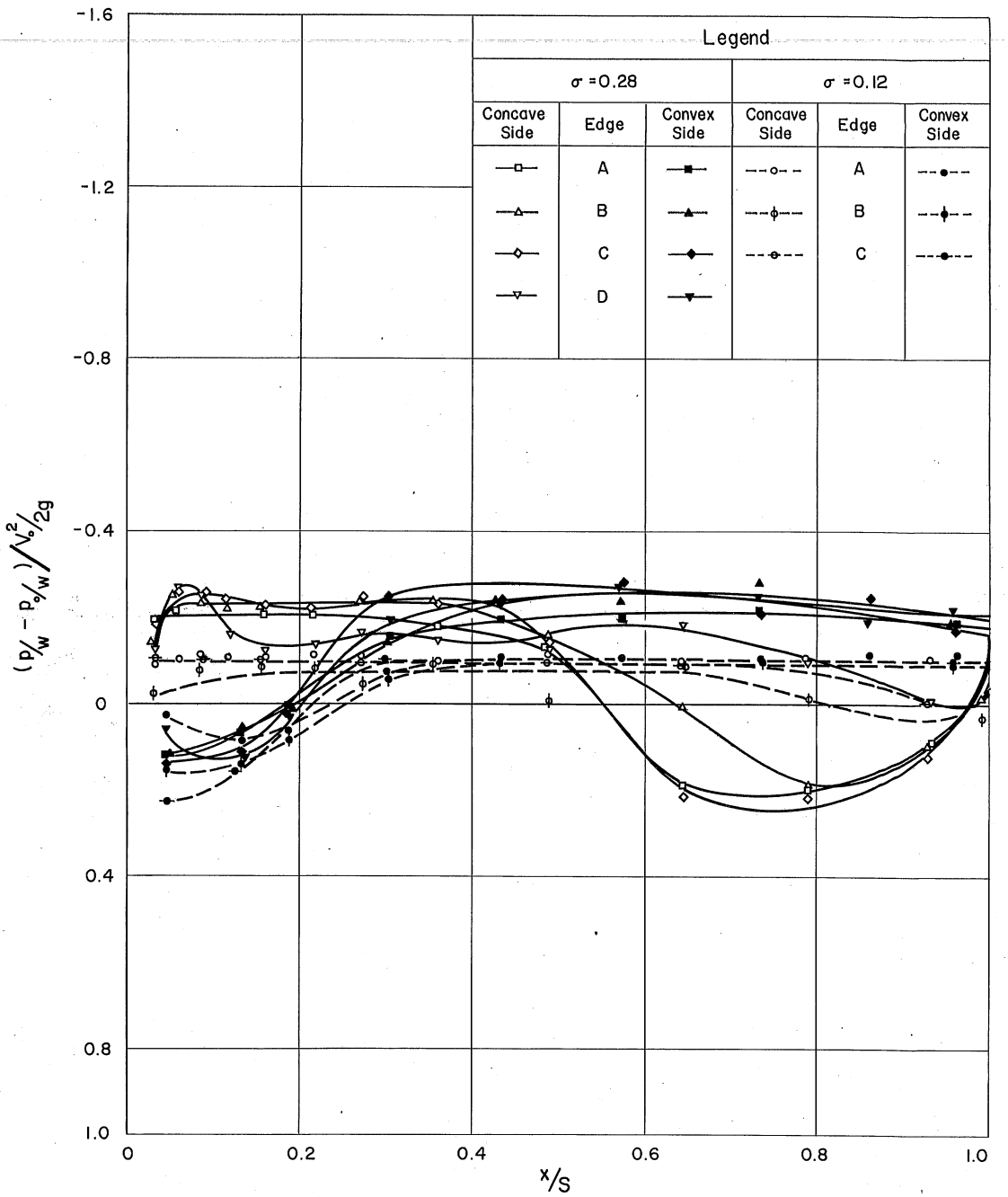

Fig. 22 – Measured Pressure Distributions, Alternate Edge Types, $\alpha' = 0$

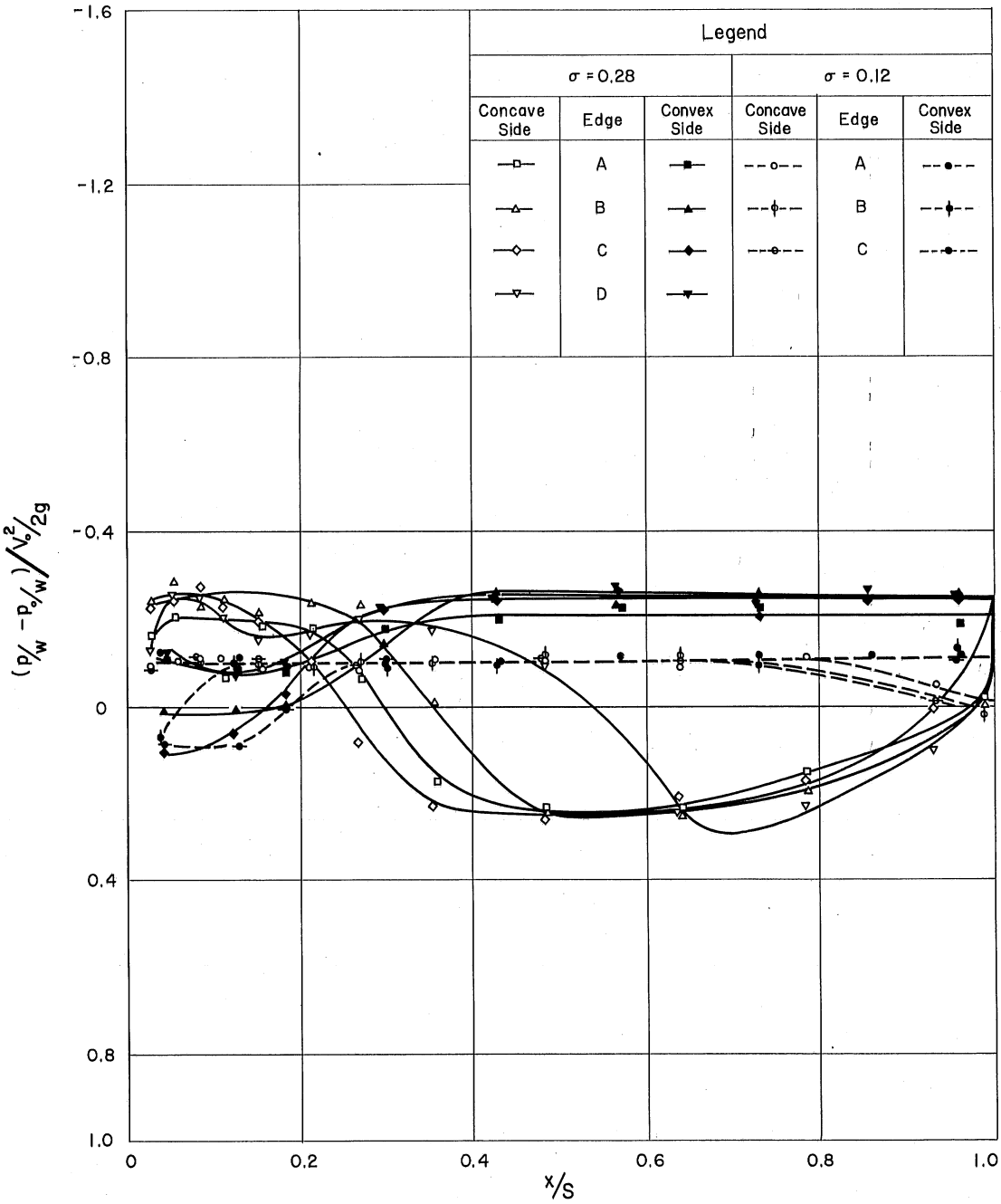

Fig. 23 - Measured Pressure Distributions, Alternate Edge Types, $\alpha' = 2$

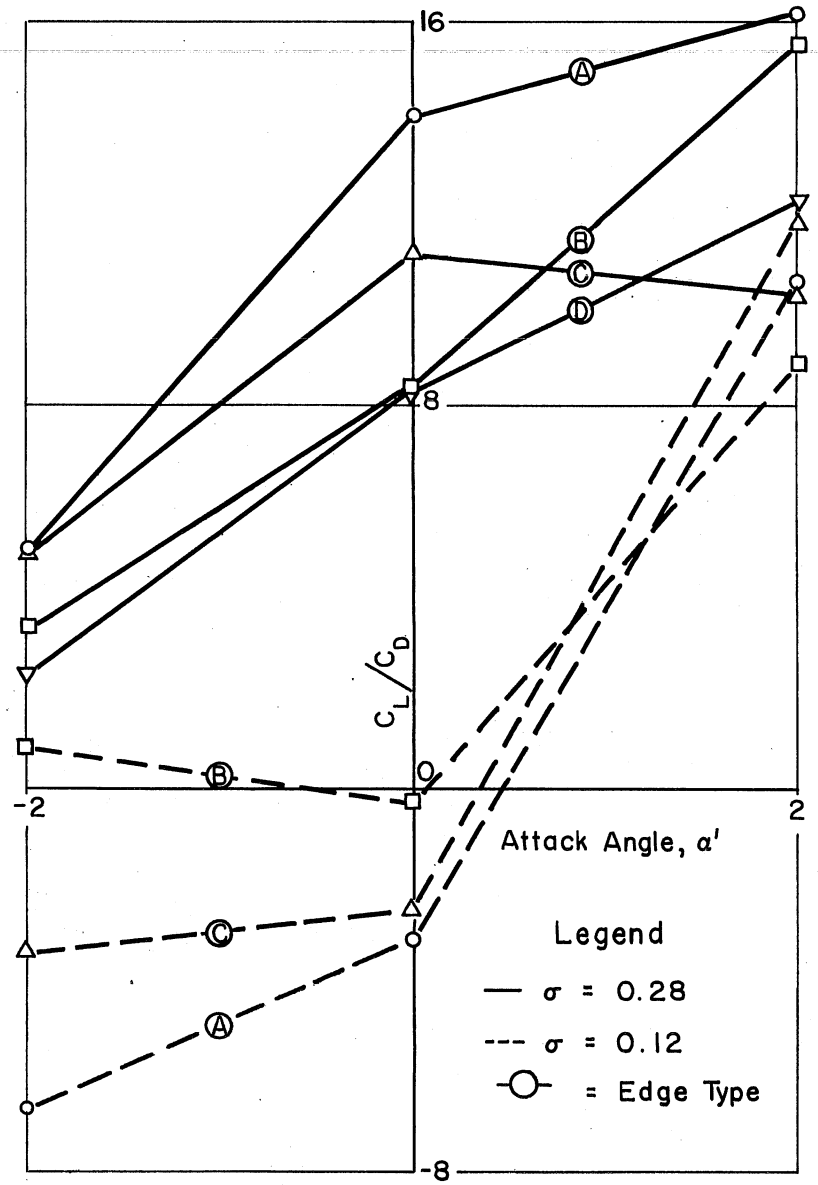

Fig. 24 - Comparative C_L/C_D Ratios for Alternate Edge Types

DISTRIBUTION LIST FOR PROJECT REPORT NO. 52
of the St. Anthony Falls Hydraulic Laboratory

Copies	Organization
14	Chief of Naval Research, Department of the Navy, Washington 25, D. C., for distribution as follows: 12 - Code 438 1 - Code 465 1 - Code 466
1	Commanding Officer, Office of Naval Research, Branch Office, The John Crerar Library Building, 86 East Randolph Street, Chicago 1, Illinois.
1	Commanding Officer, Office of Naval Research, Branch Office, 346 Broadway, New York 13, New York.
1	Commanding Officer, Office of Naval Research, Branch Office, 1030 East Green Street, Pasadena 1, California.
2	Commanding Officer, Office of Naval Research, Navy #100, Fleet Post Office, New York, New York., Attn: Dr. Julian Cole.
2	Director, Naval Research Laboratory, Washington 25, D. C., Attn: Code 2021.
1	Chief of Naval Operations, Department of the Navy, Washington 25, D. C.
1	Chief, Bureau of Aeronautics, Department of the Navy, Washington 25, D. C., Attn: Code RS-3 (Mr. F. W. S. Locke).
3	Chief, Bureau of Ordnance, Department of the Navy, Washington 25, D. C., for distribution as follows: 1 - Capt. E. B. Hooper (Code RE) 1 - Mr. J. D. Nicolaides (Code ReO3) 1 - Capt. T. S. Burdick (Code ReU)
4	Chief, Bureau of Ships, Department of the Navy, Washington 25, D. C., for distribution as follows: 1 - Radm A. M. Morgan (Code 300) 1 - Capt. J. S. Bethea (Code 410) 1 - Capt. J. H. McQuilkin (Code 420) 1 - Mr. R. B. Couch (Code 440)
1	Chief, Bureau of Yards and Docks, Department of the Navy, Washington 25, D. C., Attn: CDR A. S. Klay, Research Division.
1	Commandant, U. S. Marine Corps, Department of the Navy, Washington 25, D. C., Attn: Asst. Chief of Staff, G-3.
5	Commanding Officer and Director, David Taylor Model Basin, Carderock, Maryland, for distribution as follows:

Copies	Organization
	1 - Library (Code 142) 1 - Dr. F. H. Todd (Code 500) 1 - Mr. A. Tachmindji (Code 526) 1 - Dr. M. St. Denis (Code 580) 1 - Mr. M. S. Macovsky (Code 591)
1	Commander, U. S. Naval Ordnance Laboratory, White Oak, Maryland, Attn: Mr. L. D. Fisher, Underwater Ordnance Department.
1	Commander, Naval Ordnance Test Station, 3202 E. Foothill Blvd. Pasadena, California, Attn: Head, Underwater Ordnance Department.
1	Superintendent, U. S. Naval Postgraduate School, Monterey, California.
1	Director of Research, National Advisory Committee for Aeronautics, 1512 H Street, N. W., Washington 25, D. C.
1	Director, Langley Aeronautical Laboratory, National Advisory Committee for Aeronautics, Langley Field, Virginia, Attn: Mr. J. B. Parkinson, Hydrodynamics Division.
1	Commander, Air Force Office of Scientific Research, Tempo T, 14th and Constitution, Washington 25, D. C., Attn: Mechanics Division.
1	Office of Ordnance Research, Department of the Army, Washington 25, D. C.
1	Office of the Chief of Engineers, Department of the Army, Gravelly Point, Washington 25, D. C.
1	Chief of Transportation, Department of the Army, Washington 25, D. C.
1	Dr. J. H. McMillen, Director, National Science Foundation, 1520 H Street, N. W., Washington, D. C.
1	Director, National Bureau of Standards, Washington 25, D. C., Attn: Fluid Mechanics Division, Dr. G. B. Schubauer.
4	California Institute of Technology, Pasadena 4, California, via Commanding Officer, Office of Naval Research Branch Office, 1030 East Green Street, Pasadena 1, California, for distribution as follows: 1 - Dean F. Lindvall, Hydrodynamics Laboratory 1 - Prof. M. S. Plesset 1 - Prof. A. Acosta 1 - Prof. T. Wu
1	University of California, Berkeley 4, California, via Office of Naval Research, Resident Representative, University of California, Room 201 Building T-9, Berkeley 4, California, Attn: Department of Engineering, Prof. H. A. Schade.

Copies	Organization
1	Iowa Institute of Hydraulic Research, State University of Iowa, Iowa City, Iowa, via Headquarters Fifth Army, 1660 E. Hyde Park Blvd., Chicago 15, Illinois, Attn: Dr. H. Rouse, Director.
1	Applied Physics Laboratory, Johns Hopkins University, 8621 Georgia Avenue, Silver Spring, Maryland, via Naval Inspector of Ordnance, Johns Hopkins University, 8621 Georgia Avenue, Silver Spring, Maryland, Attn: Dr. F. Frenkiel.
1	Massachusetts Institute of Technology, Cambridge 39, Massachusetts, via Commanding Officer, Office of Naval Research Branch Office, 495 Summer Street, Boston 10, Massachusetts, Attn: Department of Civil Engineering, Prof. A. T. Ippen.
2	University of Michigan, Ann Arbor, Michigan, via Mobile Air Materiel Area, Brookley Air Force Base, Alabama, for distribution as follows: 1 - Engineering Research Institute, Prof. F. Folsom, Director 1 - Department of Civil Engineering, Prof. V. Streeter
1	University of Minnesota, Minneapolis 14, Minnesota, via Oklahoma City Air Materiel Area, Tinker Air Force Base, Oklahoma City, Oklahoma, Attn: St. Anthony Falls Hydraulic Laboratory, Prof. L. G. Straub, Director.
1	University of Notre Dame, Notre Dame, Indiana, via Mobile Air Materiel Area, Brookley Air Force Base, Alabama, Attn: College of Engineering, Prof. A. G. Strandhagen.
2	Pennsylvania State University, University Park, Pennsylvania, via Office of Naval Research, Resident Representative, University of Pittsburgh, 303 Thaw Hall, Pittsburgh, Pennsylvania, Attn: Ordnance Research Laboratory, for distribution as follows: 1 - Dr. G. Quarles, Director 1 - Prof. G. F. Wislicenus
1	Stanford University, Stanford, California, via Commanding Officer, Office of Naval Research Branch Office, 1000 Geary Street, San Francisco 9, California, Attn: Department of Mathematics, Prof. P. Garabedian.
3	Stevens Institute of Technology, 711 Hudson Street, Hoboken, New Jersey, via Commanding Officer, Office of Naval Research Branch Office, 346 Broadway, New York 13, New York, for distribution as follows: 1 - Dr. K. S. M. Davidson 1 - Dr. J. Breslin 1 - Dr. P. Kaplan Attn: President J. H. Davis, Experimental Towing Tank.
1	Woods Hole Oceanographic Institute, Woods Hole, Massachusetts, via Commanding Officer, Office of Naval Research Branch Office, 495 Summer Street, Boston 10, Massachusetts, Attn: Dr. C. Iselin.

Copies	Organization
1	Aerojet General Corporation, 6352 North Irwindale Avenue, Azusa, California, via Bureau of Aeronautics Representative, Aerojet General Corporation, 6352 North Irwindale Avenue, Azusa, California, Attn: Mr. C. Gongwer.
1	General Dynamics Corporation, Convair Division, 3302 Pacific Highway, San Diego 12, California, via Assistant Industrial Manager, U. S. Naval Station, San Diego 36, California, Attn: Mr. H. Brooks.
1	The Glenn L. Martin Company, Middle River, Baltimore 3, Maryland, via Bureau of Aeronautics Representative, Glenn L. Martin Company, Middle River, Baltimore 3, Maryland, Attn: Mr. J. Pierson.
1	Grumman Aircraft Engineering Corporation, Bethpage, Long Island, New York, via Bureau of Aeronautics Representative, Grumman Aircraft Engineering Corporation, Bethpage, Long Island, New York.
1	Edo Corporation, College Point, Long Island, New York, via Bureau of Aeronautics Representative, Kollsman Instrument Corporation, Elmhurst, Long Island, New York, Attn: Mr. S. Fenn.
1	Propulsion Research Corporation, 1860 Franklin Street, Santa Monica, California, via San Bernardino Air Materiel Area, Norton Air Force Base, California.
1	Gibbs and Cox, Inc., 21 West Street, New York 6, New York, via Supervisor of Shipbuilding and Naval Inspector of Ordnance, 139 Centre Street, New York 6, New York.
1	Dynamic Developments Corporation, St. Marks Lane, Islip, Long Island, New York, via Inspector of Naval Material, 250 Hudson St., New York 13, New York, Attn: Mr. W. Carl.
1	Miami Shipbuilding Corporation, 615 S. W. Second Avenue, Miami 36, Florida, via Supervisor of Shipbuilding and Naval Inspector of Ordnance, 1453 Morse Street, P. O. Box 5296, Jacksonville, Florida, Attn: Mr. P. Buhler.
1	Baker Manufacturing Company, 133 Enterprise Street, Evansville, Wisconsin, via Headquarters, Fifth Army, 1660 E. Hyde Park Blvd., Chicago 15, Illinois, Attn: Mr. J. Baker.
1	Eastern Research Group, 215 Montague Street, Brooklyn 1, New York, via Headquarters, Fifth Army, Governors Island, New York, Attn: Dr. L. Meyerhoff.